2013-01-01

Estimating Variations In Locking Depth For The Mojave Segment Of The San Andreas Fault Over The Past 1500 Years From Paleoseismic Stress Drop

Teira Solis
University of Texas at El Paso, tsolis2@miners.utep.edu

ESTIMATING VARIATIONS IN LOCKING DEPTH FOR THE MOJAVE SEGMENT OF THE SAN ANDREAS FAULT OVER THE PAST 1500 YEARS FROM PALEOSEISMIC STRESS DROP

TEIRA P. SOLIS

Department of Geological Sciences

APPROVED:

Bridget Smith-Konter, Ph.D., Chair

Diane I. Doser, Ph.D.

Terry L. Pavlis, Ph.D.

Eric A. Hagedorn, Ph.D.

Benjamin Flores, Ph.D.
Dean of the Graduate School

"To a geologist, stones are richly illustrated texts, telling gothic tales of scorching heat, violent tempests, endurance, cataclysm, and reincarnation. Over more than 4 billion years the planet has unintentionally kept a rich and idiosyncratic journal of its past."

Reading the Rocks: The Autobiography of the Earth
Marcia Bjornerud

ESTIMATING VARIATIONS IN LOCKING DEPTH FOR THE MOJAVE SEGMENT OF THE SAN ANDREAS FAULT OVER THE PAST 1500 YEARS FROM PALEOSEISMIC STRESS DROP

by

TEIRA SOLIS

THESIS

Presented to the Faculty of the Graduate School of

The University of Texas at El Paso

in Partial Fulfillment

of the Requirements

for the Degree of

MASTERS IN SCIENCE IN GEOPHYSICS

Department of Geological Sciences

THE UNIVERSITY OF TEXAS AT EL PASO

August 2013

Acknowledgements

Many people helped me along the way to achieve this point in my life. Life has certainly not been easy for me this past decade but choosing to go back to school and staying until the end has been one of the best decisions in my life. A series of life-changing events have shown me that no matter what, I had to stay focused in my future and on what's important.

First and foremost, I would like to thank my Advisor Bridget Smith-Konter for believing in me and giving me the opportunity to show myself what I was capable of. Your trust in me was absolutely priceless. I would like to acknowledge my committee members for their help and guidance in this project.

Thanks to my dear friend Cecilia with whom I shared many laughs and many tears and I certainly enjoyed every minute that we got to travel together. The lab just wasn't the same after you left. Also thanks to all my friends in the Geology department that throughout the years came and went. I'm so grateful that we built friendships that will last a lifetime.

Mishita: you have showed me how strong a mother's love can be and you have set the path for me to follow. Sax: I'm eternally grateful for all the wonderful stories that defined my life… I never could tell when reality turned in to fantasy. It was all absolutely amazing to me and I miss you greatly! Sisters: Thank you for being the only ones who understood what I was saying in our own secret language *Perez-Lopezco*. We are the three luckiest girls in this planet to have had the oddest, smartest people as parents. I love you.

To my beautiful daughters: Thank you for your beautiful smile every morning and your laughs. Your unconditional love was of great help and the best kind of motivation. You made me strive to be the best example to all of you and to show you that hard work and perseverance has great rewards.

And lastly to my dear husband Salvador: Thank you for your infinite patience during all those sleepless nights and long restless days. You are my eternal love and my pillar of strength. You have been my greatest motivator and also my toughest critic… not a day goes by without thanking God for having you in my life. I love you forever.

Abstract

The most fundamental model for characterizing earthquake occurrence [*Reid*, 1910] assumes a constant stress accumulation rate on a locked fault segment, which eventually fails at a threshold stress level. While this model provides a conceptual framework for investigating the conditions that prepare a fault for failure, there is little evidence that faults rupture periodically or at a uniform threshold stress. Moreover, this model fails to explain the large differences in earthquake recurrence intervals and paleoseismic slip for segments of major fault systems: why do some faults rupture on the order of 10's of years, while others require 100's of years to accumulate substantial stress before failing in a large earthquake? Previous work has shown that the rate of stress accumulation is highly sensitive to fault locking depth, where shallowly locked faults accumulate stress at higher rates than deeply locked faults. Here we investigate the role of variable locking depth on multiple earthquake cycle stress accumulation spanning the last 1500 years. We focus on the Wrightwood paleoseismic site, located along the Mojave segment of the San Andreas Fault System. We use published slip estimates (0.5-7.0 m) [*Weldon et al.*, 2004] to simulate 14 earthquake cycles of interseismic stress accumulation, coseismic stress drop, and postseismic stress relaxation over the last 1500 years using a 4D viscoelastic deformation model with realistic fault geometry. For each earthquake cycle, we assume a constant slip rate and systematically adjust the locking depth of the Mojave segment (5-25 km) to match paleoseismic stress drop. Finally, we investigate the implications of paleoseismic stress accumulation and variable locking depth in context with present-day stress estimated along the Mojave segment of the San Andreas Fault System.

Table of Contents

Acknowledgements vi

Abstract vii

Table of Contents viii

List of Tables ix

List of Figures x

Chapter 1: San Andreas Fault System 1

1.1 Introduction 1

1.2 Motivation: Improving earthquake hazard models 5

1.3 Digging up fault histories: Paleoseismology 5

1.4 The earthquake cycle 7

1.5 Earthquake cycle stress model 9

1.6 Thesis organization 13

1.7 References 14

Chapter 2: Building earthquake recurrence cycles using paleo-event chronologies of the San Andreas Fault System over the last 2000 years 16

2.1 Introduction 16

2.2 Historic and pre-historic earthquakes of the SAFS 16

2.3 Building the SAFS paleoseismic database V2 19

2.4 Results and discussion: Paleoseismic earthquake rupture map 21

2.5 Conclusions 22

2.6 References 24

Chapter 3: Estimating variations in locking depth for the Mojave segment of the San Andreas fault over the past 1500 years from paleoseismic stress drop 27
3.1 Abstract 27
3.2 Introduction 28
3.3 Paleoseismic data 31
3.4 4-D earthquake cycle modeling 21
3.5 Estimating stress drop: Paleoseismic data and 4-D models 36
3.6 Estimating depth-dependent stress drop: data and 4-D models 40
3.7 Discussion: Variation in locking depths, stress rates and implications for seismic hazards 46
3.8 Conclusions 50
3.9 References 53

Appendix 1 A: San Andreas Fault System Paleoseismic Database Version 2 56

Appendix 2 A: Stress drop variations on the Mojave segment for the past 1500 years using a variable slip rate 64

Curriculum Vita 71

List of Tables

Table 2.1: Prehistorical SAFS earthquakes from 1000 A.D. 18
Table 2.2: Example of Paleoseismic database for the Mojave segment 21
Table 3.1: Paleoseismic data at Wrightwood, CA. 33
Table 1.A.1: SAFS PDV2 1. San Adreas fault segments 58
Table 1.A.2: SAFS PDV2 2. Imperial and Cerro Prieto faults 62
Table 1.A.3: SAFS PDV2 3. San Jacinto fault 63
Table 1.A.4: SAFS PDV2 4. Elsinore fault 64
Table 2.A.1: Data used to calculate variable slip rate for the Mojave segment 66

List of Figures

Figure 1.1: Regional map of California. 1
Figure 1.2: Map of California with historic ruptures. 4
Figure 1.3: Regional map of southern California showing the SAF at Wrightwood 7
Figure 1.4: Representation of interseismic stress accumulation and coseismic stress drop. 7
Figure 1.5: Simple earthquake recurrence models. 8
Figure 1.6: Hypothetical stress accumulation and drop 10
Figure 1.7: 2-D crustal deformation models. 12
Figure 1.8: Schematic of 3-D fault deformation model. 13
Figure 2.1: Historical earthquake ruptures of the SAF from 1800 to 2004. 18
Figure 2.3: Paleoseismic earthquake map of the SAF from 0 A.D. to 2012 A.D.. 23
Figure 3.1: Stress accumulation rate model of the southern SAF. 29
Figure 3.2: Snapshots of stress accumulation using a fixed slip rate. 34
Figure 3.3: Time-series of model stress accumulation and stress drop (10 year sample). 35
Figure 3.4: Mojave segment fault dimensions used to calculate stress drop. 36
Figure 3.5: Paleoseismic stress drop and estimated stress accumulation. 38
Figure 3.6: Paleoseismic stress drop vs. recurrence interval. 39
Figure 3.7: Estimated paleoseismic stress drop as a function of locking depth. 41
Figure 3.8: Modeled stress drop for the 1812 and 1857 events ad different locking depths. 42
Figure 3.9: Model and paleoseismic slip-derives stress drop as a funtion of locking depth. 43
Figure 3.10: Comparison of stress drop from model and paleseismic data at 5, 15, and 25 km. ..45
Figure 3.11: Best fitting locking depth per earthquake cycle for the Mojave segment. 47
Figure 1.A.1: Regional map of southern SAF and names of segments. 56
Figure 2.A.1: Snapshots of stress accumulation using a variable slip rate. 66
Figure 2.A.2: Paleoseismic slip-derived stress drop. L, W, and LW relationships. 68
Figure 2.A.3: Data vs. Model stress drop estimates. L, W, and LW relationships 70

Chapter 1: San Andreas Fault System

1.1 Introduction

The San Andreas Fault System (SAFS) in California is considered the primary tectonic boundary between the North American and the Pacific plates in southwestern North America (Figure 1.1). This transform margin developed in western California approximately 29 Ma and accommodates 35-50 mm/yr of slip along its ~1500 km of length [*Atwater and Molnar*., 1973]. Over the last 1000 years it is estimated that at least 70 major earthquakes (M_w>6.0) have ruptured the SAFS, with 50% of these events occurring in the last 200 years [*WGCEP*, 2007]. Small earthquake events also add to the regional seismicity of the SAFS plate boundary; southern California endures about 10,000 earthquakes each year, with most of these of M_w< 3.0, and only about 15-20 of M_w> 4.0 [earthquake.usgs.gov].

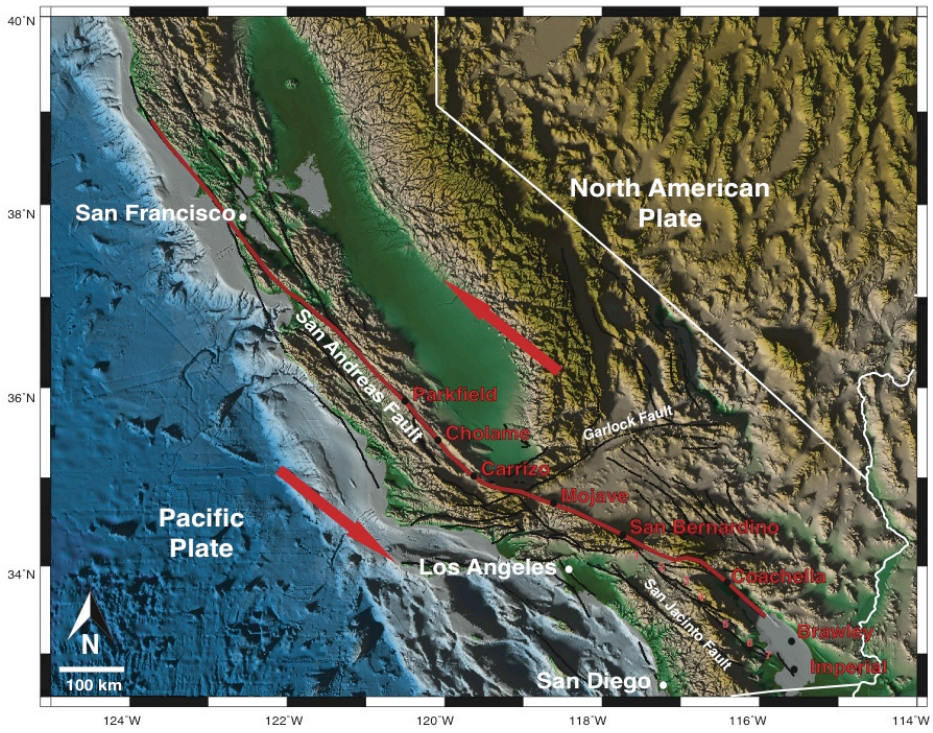

Figure 1.1: Regional map of California showing the North American and the Pacific plates, as well as their relative direction of motion (red arrows). The extent of the SAFS is traced in red with names of individual segments provided.

Despite the large amounts of data generated from one of the most thoroughly studied faults on the planet, there are still many unanswered questions regarding segmentation, rupture patterns and characteristics of large earthquakes [*Grant et al.,* 2002]: What is the average repeat time of earthquakes on a fault? Is the amount of slip and length of a fault rupture generated by an earthquake related to the magnitude? [*Wallace,* 1970]. Do great earthquake ruptures terminate at the segment boundaries? [*Wiss, et al.*, 1995]. Why do some faults rupture on the order of 10s of years, while others require 100s of years to accumulate substantial stress before failing in a large earthquake? [*Smith-Konter and Sandwell*, 2009]. These major questions about earthquake recurrence and size provide ample motivation to further evaluate the role of stress/strain accumulation and release throughout multiple earthquake cycles along the SAFS.

In 1910, Harry Reid proposed the "Elastic Rebound Theory" based on observations of the damage after the 1906 San Francisco earthquake [*Reid*, 1910]. This theory postulates that crustal stresses from large-scale shearing motions cause strain to accumulate. When this strain reaches a critical threshold, sliding occurs, releasing the elastic strain energy (or stress drop). Whether this process releases the strain (or stress) in its entirety or only partially is still unknown. However, as soon as this occurs, the strain begins to accumulate again, leading to a complete cycle of accumulation and release that will repeat many times over the life of a fault.

It is assumed widely that great earthquakes (M_w>6.0) in California occur with some degree of regularity [*Weldon et al.,* 2004]. However, based on evidence gathered so far, we cannot considered these occurrences periodic, making the efforts of modeling and forecasting earthquakes a difficult task. The differences in the geometry of the individual segments along the SAFS (discussed further in Chapter 2) and the interactions with the many other large faults in the region (Figure 1) add to the complexity of building sophisticated computer models capable of simulating realistic scenarios of earthquake behavior. Furthermore, a detailed and comprehensive chronology of multiple earthquake

events (for a common reference location) extending back in time for 100s of years is critical component of earthquake cycle simulations. Such paleoseismic data are limited, however much progress has been made over the last 20 years to extract this type of information from multiple study sites along the SAFS [*Petersen et al*., 1994; *Grant et al*., 1994; *Weldon et al*., 2004; *McGill et al*., 2008; *Toke et al*., 2009].

The two most recent large earthquakes of the SAFS occurred in the northern and central sections in 1906 (M 7.8) and 1857 (M 7.9), respectively (Figure 1.2). The southern portion, however, has not experienced any major seismic activity in the last ~250 years. This and the recent significantly higher frequency of moderate earthquakes leads us to a widely held opinion that this part of the SAFS is in a late stage of its earthquake cycle [*Fialko,* 2006]. Historically, increased seismic activity on a fault after a long period of quiescence has been associated with large (Mw>7.0) earthquakes; but longer records of seismic behavior would allow more robust estimates of these recurrence intervals [*Fialko,* 2006]. Like the southern section of the SAFS, the central section has also experienced a period of relative quiescence. Significant earthquake activity has been absent for over 150 years along the section of the SAFS that ruptured in 1857. Average earthquake repeat times here are ~ 105 years (31-165 yrs for individual intervals) [*Weldon et al*., 2004] , thus we infer this region of the SAFS to also be quite hazardous.

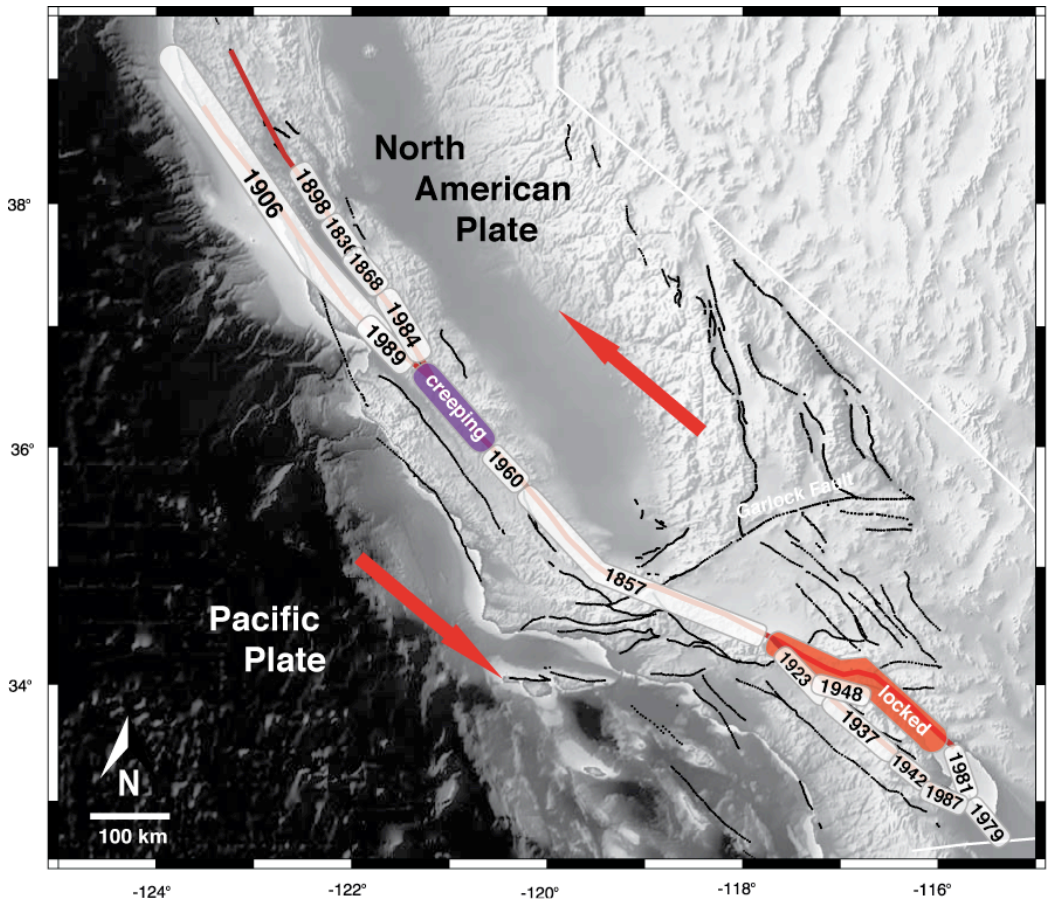

Figure 1.2. Modified from *Sandwell and Smith* [2007]. Map of California showing the approximate extent of historic ruptures along the entire SAFS.

The main objective of this research is to investigate the relationship between stress drop variations and the spatial and temporal occurrence of major earthquakes along the SAFS. To achieve this task, it is necessary to construct a comprehensive paleoseismic database with abundant observation points spanning long periods of time (Chapter 2). While our primary research focus is the Mojave segment of the SAFS (Chapter 3), we initially began this study by compiling paleoseismic data for all segments of the SAFS to assess which segments could provide optimal information about multiple earthquake cycles. These technical results are reported in the following chapters and a more general background about earthquake cycle models and data are provided in the following sections.

1.2 MOTIVATION: IMPROVING EARTHQUAKE HAZARD MODELS

Knowledge of the spatial and temporal behavior of earthquake stress in California is essential for reliable earthquake hazard evaluations and mitigation [*Sieh*, 1990]. Earthquake hazard analyses are extremely important for major cities located along active faults. Industrial facilities and skyscrapers that are usually found in these mega-cities are prone to failure causing massive amounts of human loss [*Mohammadioun*, 2001]. In particular, the southern SAFS is a region home to over 10 million people, the site of large earthquakes in the past, and has had an absence of a major seismic activity over the past 1-3 centuries. Moreover, a critical goal of NSF's EarthScope project is *"The ability to better forecast and respond to hazards and mitigate the associated risks*" [*Williams et al.,* 2010].

Hazard models are heavily relied-on to make important public policy decisions. They are required to use "the best available science" [*Petersen*, 2008] intended for the use by decision makers in federal, state and local governments, as well as agencies in the private sector. Scientists and engineers build and use these maps in effort to prevent or mitigate disasters at the same time as educating the general population. Government agencies such as the USGS also provide updated information of seismic hazards nationwide. (http://earthquake.usgs.gov/hazards/products/tdep/petersenSRL.pdf).

1.3 DIGGING UP FAULT HISTORIES: PALEOSEISMOLOGY

A detailed chronology of earthquake events extending back in time for 100s of years is critical component of earthquake hazard modeling. Paleoseismology is the study of such events, or prehistoric earthquakes, which focuses on identifying their location, magnitude and amount of displacement [*McCalpin*, 1996]. Paleoseismology has become an important tool in characterizing sequences of prehistoric earthquakes over large periods of time and has helped improve our understanding of current patterns in seismic activity around the world. Because paleo-earthquakes occurred prior to the modern instrumentation era, paleoseismic techniques depend highly on field investigation methods to provide spatial and temporal information of past fault ruptures. The data gathered from these sites is catalogued

as “primary” or “non-primary” data. The primary data are direct measurements (i.e., surface and near-surface slip, location of fault trace, sense of motion, etc.) that require minimal interpretation, but because primary data are available at very few locations, these data are often extrapolated and interpreted to extend the coverage for applications such as seismic hazard assessment. Non-primary data include characteristic and estimated recurrence intervals, magnitudes of prehistoric earthquakes, and all the properties that define individual fault segments [*Grant et al*., 2004].

Although many assumptions have to be made, paleoseismic-derived events are based on real data and careful comparison with similar work and historic records [*Bilham*, 2009]. A variety of dating methods are used to determine a range of dates for each paleoseismic earthquake event. Carbon dating, tree-ring dating, earthquake induced subsidence and sea-level changes are the techniques most commonly used. It is important to note that the paleoseismic record is often a record of large (M>6) or great (M>7.8) earthquakes. Features formed during an earthquake rupture (landslides or fault scarps) are subject to erosion, deposition and other non-seismic events over extended periods of time that erase them from the surface. Any geologic evidence created during smaller-magnitude earthquakes is rarely preserved or may have not created any evidence at all [*McCalpin,* 1996].

Numerous studies spanning the entire SAFS have been conducted in an attempt to document a sequence of events that could potentially lead to accurate earthquake forecasting [*Grant et al.,* 1994; *Topozzada,* 2002; *Meltzner et al*., 2006; *van der Woerd*, 2006; *Scharer et al*., 2007]. Figure 1.3 shows an example of some paleoseismic sites along the Mojave segment [*Sharer et al.,* 2007], however paleoseismic studies have been conducted on well over 50 sites along the entire SAFS to obtain earthquake histories for other active fault segments. A more in-depth analysis of these data for the entire SAFS, from a paleoseismic perspective, is discussed in Chapter 2.

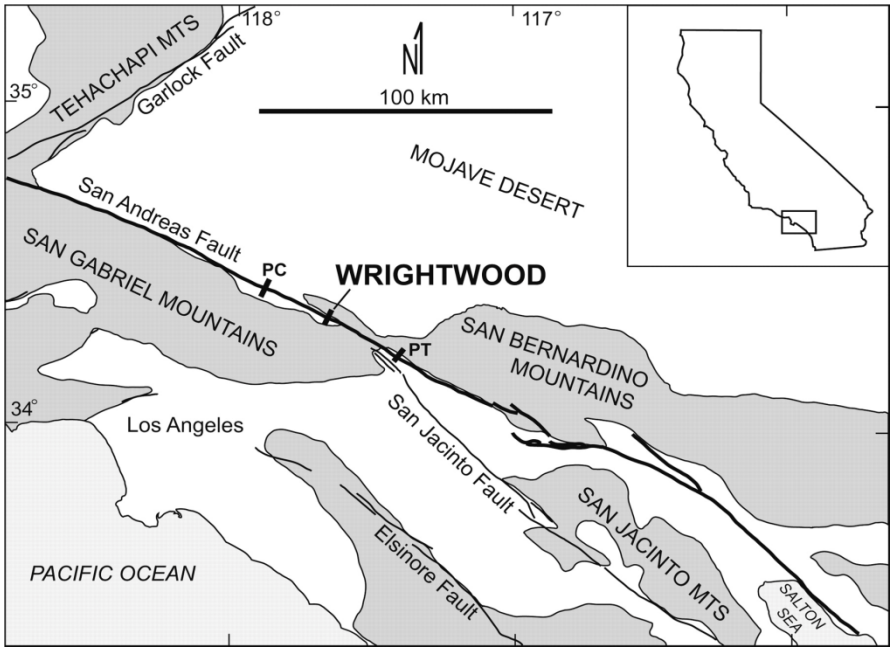

Figure 1.3: Regional map of southern California showing the San Andreas fault at Wrightwood, Pallet Creek (PC), and Pitman Canyon (PT) paleoseismic sites. General location shown on inset map of California [*From Scharer et al*., 2007].

1.4 THE EARTHQUAKE CYCLE

The earthquake cycle can be defined as a simplified representation of stress accumulation on a fault over 10s to 100s of years (called the interseismic stage) and a instantaneous stress drop (called the coseismic stage) that results after each earthquake (Figure 1.4).

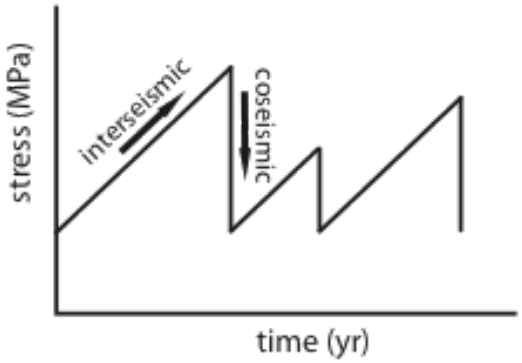

Figure 1.4: Representation of stress accumulation during the interseismic stage and stress drop during the coseismic stage.

A "periodic", or "characteristic", earthquake cycle model interprets Reid's concept of successive earthquakes [*Stein and Wysession*, 2003] having similar stress drop amounts after the stress reaches a critical threshold [*Scholz*, 1990]; however, evidence shows that the recurrence of big earthquakes on single fault segments are not periodic in time nor do they have equivalent amounts of stress drop [*Murray and Segall*, 2002; *Weldon et. al*, 2004]. The "time-predictable" version of this model (Figure 1.5b), for example, assumes the strength of the fault is constant but the stress drop, after reaching a critical threshold, will vary. Alternatively, the "slip-predictable" version of this model (Figure 1.5c) assumes that the accumulated stress level before a slip event is variable, but that the stress will drop to zero and the time this accumulation will require is determined by the slip rate individual to each fault segment [*Murray and Segall*, 2002; *Weldon et al*., 2004]. Based on evidence from several studies, it is more likely that the time or slip predictable models represent a more realistic representation of true earthquake cycles than that of the characteristic model [*Weldon et al*., 2004].

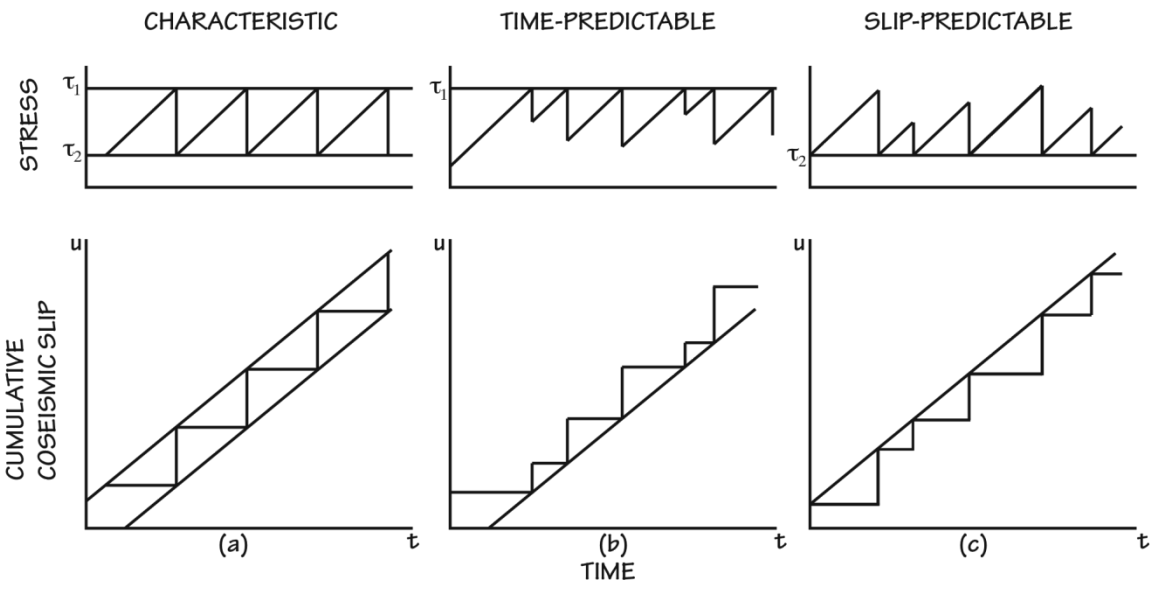

Figure 1.5: Simple earthquake recurrence models: (a) characteristic, or perfectly periodic, (b) time predictable, (c) slip-predictable from [*Scholz*, 1990].

In this study, we utilize different aspects of the earthquake cycle to investigate interseismic stress accumulation, coseismic stress drop and post-seismic (a short period of time - on the order of a few months to years following the earthquake) relaxation. During the interseismic stage, stress accumulates in the shallow locked zone of the fault due to forces from deep slip below. During the coseismic stage, this accumulated stress in the shallow locked zone is suddenly released, resulting in fault slip, or offset (an earthquake). During the postseismic stage, stresses below the locked zone readjust and relax, sometimes causing a phenomenon know as stress shadows [*Harris and Simpson,* 1996, 1998; Harris, 1998], before the cycle repeats itself.

1.5 EARTHQUAKE CYCLE STRESS MODELS

Using sophisticated computer models, we can explore earthquake scenarios that span several thousands years, or multiple earthquake cycles. Modern geodetic measurements (i.e., the EarthScope Plate Boundary Observatory (PBO)) provide a present day estimate of the plate boundary velocity field of the SAFS, which can then be ingested into a physical model to calculate strain rate and stress fields, assuming a specific rheology of the crust. When combined with paleoseismic chronologies of major earthquakes along the SAFS [i.e., *Grant*, 2002; *Weldon et al*., 2004; *Toké et al*., 2006], a near-complete earthquake cycle model can be constructed that simulates interseismic stress accumulation (at rates consistent with GPS velocities), coseismic stress drop (consistent with earthquake rupture displacements) (Figure 1.6), and post-seismic relaxation (consistent with a timescale determined by an assumed rheology). With these types of models we can begin to understand the earthquake cycle mechanics that govern variable stress drop processes. However, precise knowledge of parameters such as fault locking depth, slip rate, and rupture lengths are also necessary for obtaining accurate estimates of tectonic stress accumulation, stress drop, and earthquake magnitudes that may be generated along the SAFS.

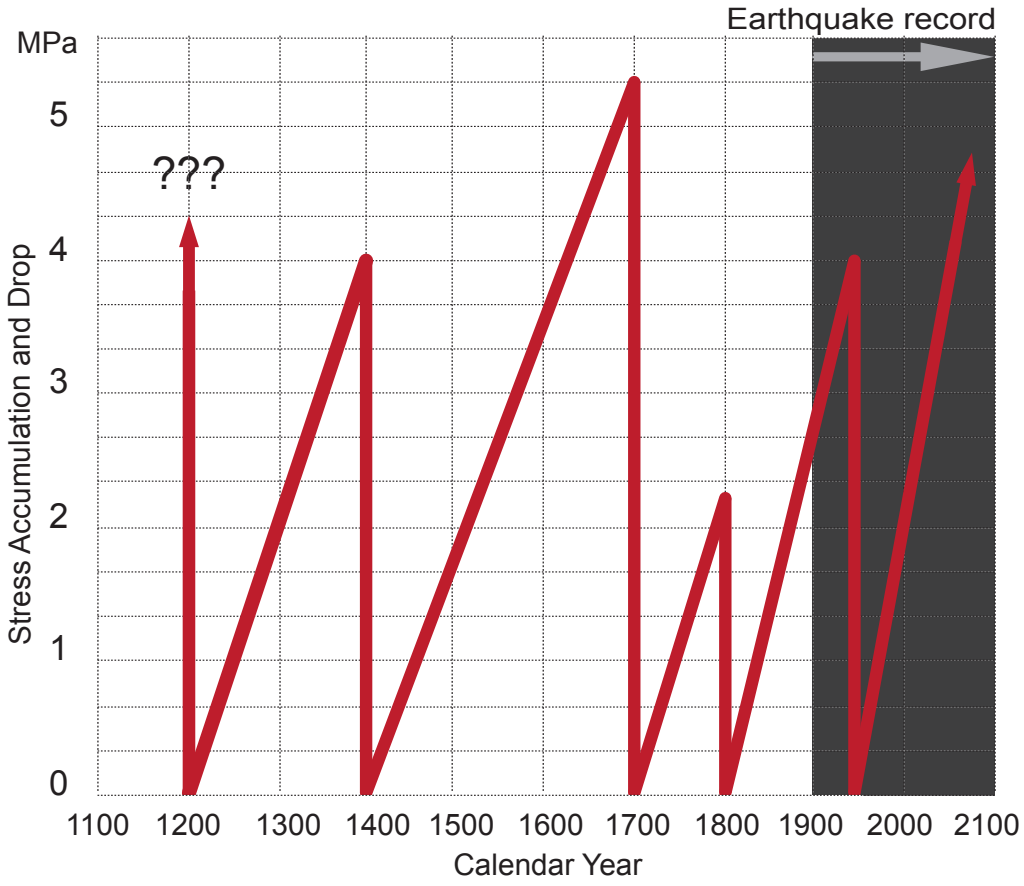

Figure 1.6. Diagram showing a hypothetical stress accumulation and drop sequence of a fault segment over the past 1000 years. The gray box represents the time span of the earthquake record that can be determined using modern instrumentation. The white area simulates a time span that might be studied using paleoseismology to complete the earthquake record.

Analytic models can provide descriptions of fault motions in 2 and 3 dimensions. A basic 2-D analytic model, for example, can simulate: 1) interseismic deformation from a shallowly locked fault that is freely slipping (accommodating long-term plate motion at a constant slip rate) below the locked portion, or 2) coseismic deformation resulting from sudden stress release along the shallowly locked fault. Equations 1.1 and 1.2 below provide mathematical descriptions for these distinct fault behaviors within a homogeneous elastic half space, defined by slip between depths d_1 and d_2 [*Weertman,* 1964], where v is the displacement (or velocity), V_o is the slip (or slip rate), x is the horizontal distance across the fault plane, and d_1 and d_2 are the lower and upper depths describing the slipping region, respectively:

$$v(x) = \frac{v_o}{\pi}\left[\tan^{-1}\left(\frac{x}{d_2}\right) - \tan^{-1}\left(\frac{x}{d_1}\right)\right] \quad (1.1)$$

$$v(x) = \frac{-v_o}{\pi}\left[\tan^{-1}\left(\frac{d_2}{x}\right) - \tan^{-1}\left(\frac{d_1}{x}\right)\right] \quad (1.2)$$

These 2-D equations simulate how the surface displacement or velocity varies with horizontal distance from the fault. Equation 1.1 describes deep slip motion during the interseismic stage (Figure 1.7a); equation 1.2 describes the shallow displacement of a fault during the cosesimic stage (Figure 1.7b,). A simple arctangent function transitioning across the fault plane is represented by the interseismic velocity pattern (Figure 1.7a). The coseismic slip pattern (Figure 1.7b) supplements the slip deficit near the fault plane. The derivative of these equations provides deformation in terms of strain (ε) or strain accumulation rate (Figure 1.7c) and subsequent strain drop (Figure 1.7d). Assuming a homogeneous, isotropic medium, these results can also be interpreted in terms of shear stress (or stress rate), which is simply strain multiplied by the shear modulus, μ:

$$\tau = \mu * e \quad (1.3)$$

Figure 1.7 also shows the behavior of the 2-D models at different locking depths. For the interseismic model (a), a shallow locking depth (blue line, 5 km) will yield a sharper interseismic velocity step across the fault than a deep locking depth (green line, 25 km). Similarly, a shallow locking depth will produce a higher strain (or stress) accumulation rate (c) than a deeper locking depth. In terms of stress drop (d), the same pattern emerges, where a shallow locking depth will produce a higher strain release (or stress drop) than a deep locking depth.

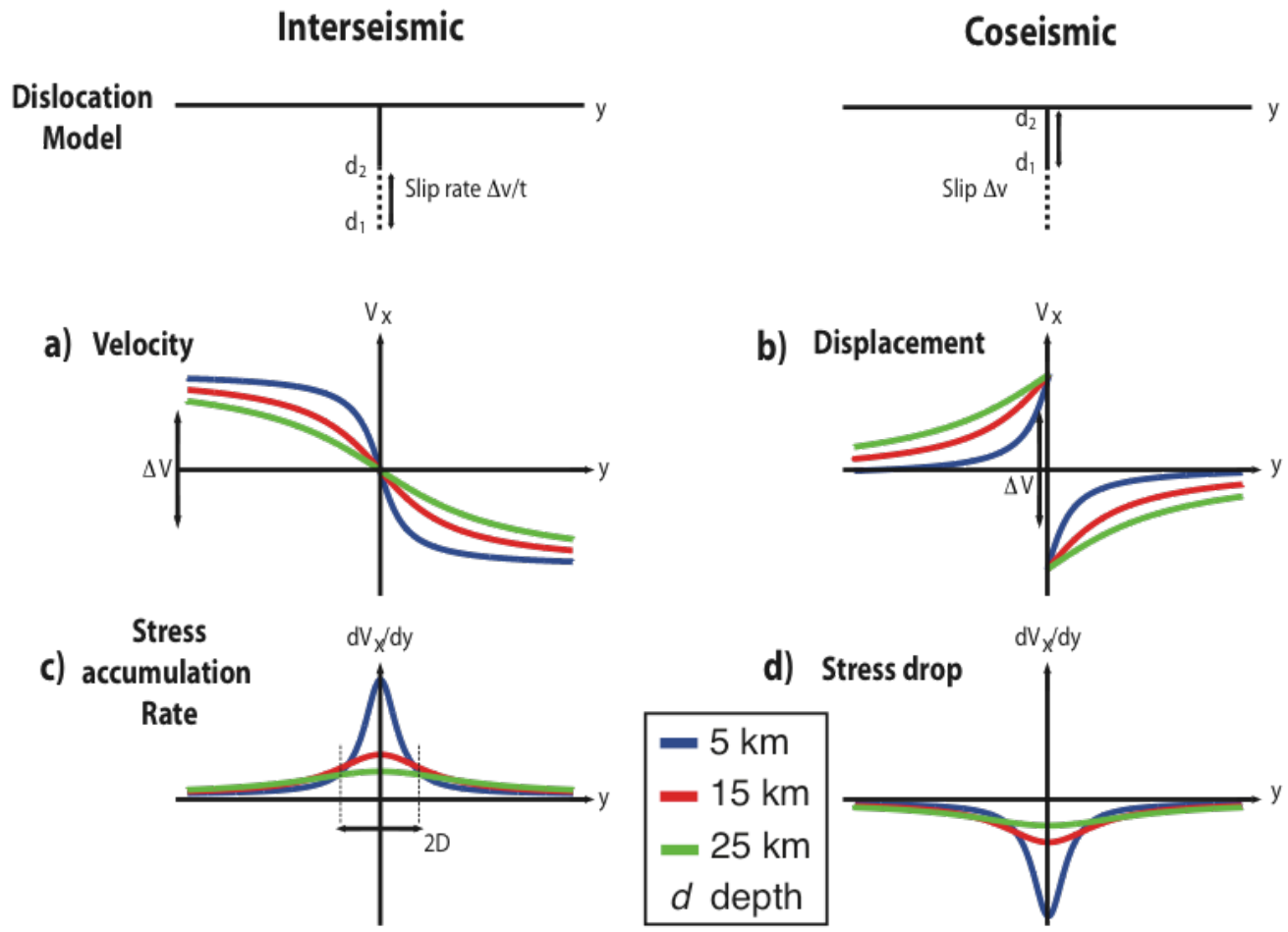

Figure 1.7: 2-D crustal deformation models simulating interseismic and coseismic earthquake cycle behaviors. (a,c) 2-D interseismic model representing surface velocity and strain accumulation rate of a locked fault with deep interseismic slip below depth d (d_2 for this model). (b,d) 2-D coseismic model representing displacement of a fault locked down to depth d (d_1 for this model) and strain release. Blue curve represents model behavior for a locking depth d of 5 km. Red curve represents model behavior using a locking depth of 15 km. The green curve represents model behavior using a locking depth of 25 km. Figure adopted and modified from *Thatcher* [1986].

3-D models of crustal deformation and stress/strain [i.e., *Smith and Sandwell*, 2003] generate the same first-order behavior demonstrated by the above 2-D models, however these also account for variations that arise from finite and curved fault geometry. 4-D models (time-dependent) [i.e., *Smith and Sandwell*, 2004; 2006] can simulate multiple earthquake cycles of interseismic stress accumulation, coseismic stress drop, and postseismic stress relaxation. The Smith and Sandwell 4-D model (a semi-analytic computational code) is used throughout this study to simulate interseismic stress accumulation and coseismic stress drop along the SAFS. It simulates fault motion for realistic fault geometry and

requires a variety of input parameters, like thickness of the elastic plate (H), slip rate V_o, shear modulus (μ), Youngs Modulus (E), viscosity (η), and density (ρ) (Figure 1.7).

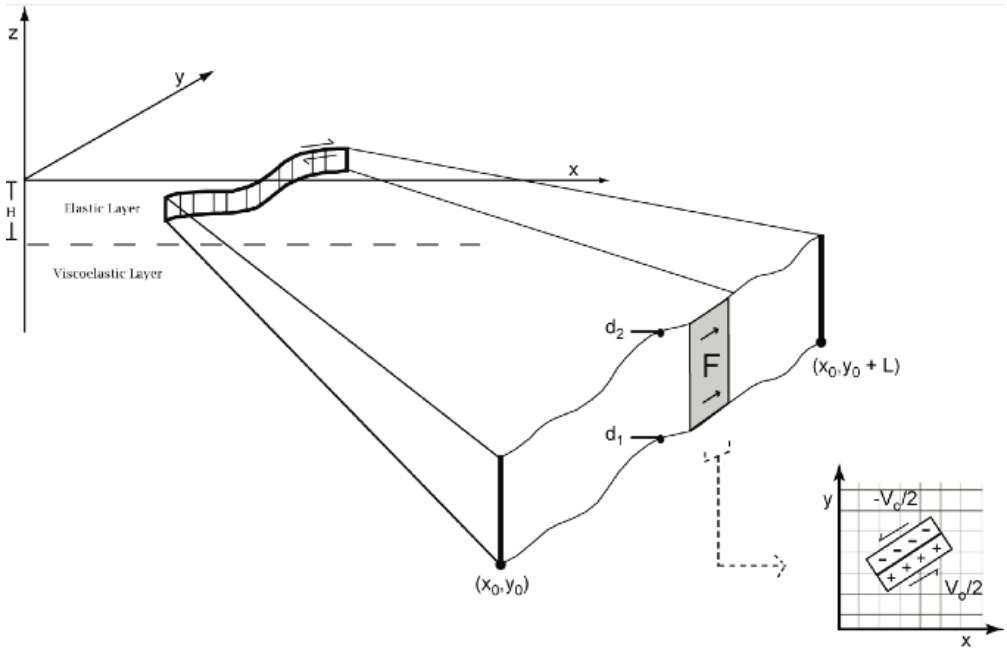

Figure 1.7: Schematic of the 3-D fault deformation model used in this study [*from Smith and Sandwell*, 2004]. This model simulates deformation due to a fault imbedded within an elastic layer overlying a linear Maxwell viscoelastic half-space with thickness elastic plate (H), slip rate V_o, shear modulus (μ), Youngs Modulus (E), viscosity (η), and density (ρ).

1.6 THESIS ORGANIZATION

The primary goal of this thesis is to investigate patterns in stress accumulation of the SAFS over multiple earthquake cycles. This will involve the compilation of new estimates of paleoseismic faulting histories explained in detail in Chapter 2 [e.g., *Weldon et al*., 2004] to determine how characteristically a fault segment behaves throughout multiple earthquake cycles. In Chapter 3, these data will then be integrated into a 4-D viscoelastic deformation model to simulate stress evolution over multiple earthquake cycles and using a variable locking depth. Chapter 3 is being prepared for publication, with additional figures provided in Appendix 2 A.

1.7 REFERENCES

Atwater, T., and Molnar, P. (1973), Relative motion of the Pacific and North American plates deduced from sea-floor spreading in the Atlantic, Indian, and South Pacific Oceans. *Stanford Univ. Publ. Geol. Sci*, *13*, 136-148.

Bilham, R. (2009), The seismic future of cities. *Bull. Earth. Eng.*, 7:839-887. doi:10.1007/s10518-009-91470.

Fialko, Y. (2006), Interseismic strain accumulation and the earthquake potential on the southern San Andreas fault system**.** *Nature* 441, 968-971.

Grant, L.B. and Sieh, K., (1994), Paleoseismic evidence of clustered earthquakes on the San Andreas fault in the Carrizo plain, California. *J. Geophys. Res.*, 99, 6819-6841.

Grant, L.B. and Lettis, W.R., (2002), Introduction to the special issue on paleoseismology of the San Andreas fault System. *Bull. Seismol. Soc. Am.,* 92, 2551-2554.

Grant, L.B. and Goul, M.M., (2004), Assimilation of paleoseismic data for earthquake simulation. *Pure and Applied Geophysics* 161, 2295-2306.

Harris, R. A., and Simpson, R. W., (1996), In the shadow of 1857-the effect of the Great Ft. Tejon Earthquake on subsequent earthquakes in southern California. *Geophysical Research Letters*, *23*(3), 229-232.

Harris, R. A. (1998), Introduction to special section: Stress triggers, stress shadows, and implications for seismic hazard. *Journal of Geophysical Research: Solid Earth)*, *103*(B10), 24347-24358

Harris, R. A., and Simpson, R. W. (1998), Suppression of large earthquakes by stress shadows: A comparison of Coulomb and rate-and-state failure. *J. Geophys. Res.: Solid Earth 103* (B10), 24439-24451.

Kanamori, H. and Allen, C.R., (1986), Earthquake repeat time and average stress drop. In: S Das, J. Boatwright and C.H. Scholz (Editors). Earthquake Source Mechanics. Am. Geophys.Union. Washington, D.C. *Geophys. Monogr.*, 37: 227-235.

Kanamori, H. (1994), Mechanics of earthquakes. *An. Rev. Earth Planet. Sci.*, 22, 207-237.

McCalpin, J. P. (1996). *Paleoseismology*. Academic Press, San Diego.

McGill, S., Weldon, R. J., and Owen, L. (2008). Preliminary slip rates along the San Bernardino strand of the San Andreas fault.

Meltzner, A.J., Rockwell T.K., and Owen, L.A. , (2006), Recent and long-term behavior of the Brawley fault zone, Imperial Valley, California: An escalation in slip rate? *Bull. Seismol. Soc. Am*, 96(6), 2304-2328.

Mohammadioun, B. and Serva, L., (2001), Stress drop, slip type, earthquake magnitude, and seismic hazard. *Bulletin of the Seism. Soc. Am.*, 91, 694–707.

Murray, J. and Segall, P, (2002), Testing time-predictable earthquake recurrence by direct measurement of strain accumulation and release. *Nature*, 419, 287-291.

Petersen, M.D., Frankel, A.D., Harmsen, S. C., Mueller, C. S., Haller, K. M., Wheeler, R. L., Wesson, R. L., Zeng, Y., Boyd, O.S., Perkins, D. M., Luco, N., Field, E. H., Wills, C. J., and Rukstales, K. S. (2008), Documentation for the 2008 update of the United States national seismic hazard maps, U.S. Geol. Surv. Open File Rep., 2008-1128, 61 pp.

Reid, H.F. (1910), The mechanism of the earthquake, The California Earthquake of April 18, 1906, report of the State Earthquake Investigation Commision, 2 Washingtn D.C.: Carnegie Institution.

Scharer, K. M., Weldon II, R. J., Fumal, T. E., and Biasi, G. P., (2007), Paleoearthquakes on the southern San Andreas fault, Wrightwood, California, 3000 to 1500 B.C.: A new method for evaluating paleoseismic evidence and earthquake horizons. *Bull. Seismol. Soc. Am.*, 97, 1054 – 1093, doi:10.1785/0120060137.

Scholz, C. H., and Cowie, P.A. (1990), Determination of total strain from faulting using slip measurements. *Nature,* 346, doi: 10.1038/346837a0.

Sieh, K. E. and Williams, P. L. (1990), Behavior of the San Andreas fault during the past 300 years. *J. Geophys. Res.*, 95, 6629-6645.

Sandwell, D.T. and Smith, B., (2007), California Earthquakes, in Glimpses of a Changing World: Views of Planet Earth from Space, M. D. King, C. L. Parkinson, K. C. Partington, and R. G. Williams, Eds., Cambridge University Press, 140-143.

Smith-Konter, B. and. Sandwell, D.T., (2009), Stress evolution of the San Andreas Fault System: Recurrence interval versus locking depth. *Geophys. Res. Lett.*, 36, doi:10.1029/2009GL037235.

Toké, N. A., Arrowsmith, J.R., Rymer, M. J., Landgraf, A., Coyan, J., Busch, M., Haddad, D., (2009), "Long-lived creep, M6 earthquakes, and a Holocene slip rate for the main trace of the San Andreas Fault at Parkfield, California" Annual Southern California Earthquake Center Meeting, Proceedings and Abstracts, vol. 19, Palm Springs, California, September 12-16th,

Van Der Woerd, J., Klinger, Y., Sieh, K., Tapponnier, P., Ryerson, F. J., and Mériaux, A. S. (2006), Long-term slip rate of the southern San Andreas fault from 10Be-26Al surface exposure dating of an offset alluvial fan. *J. Geophys. Res.*, 111(B4), B04407.

Wallace, R. E. (1970), Earthquake recurrence intervals on the San Andreas fault. *Geological Society of America Bulletin*, *81*(10), 2875-2890.

Weldon, R., Scharer, K., Fumal, T., and Biasi, G. (2004), Wrightwood and the earthquake cycle: What a long recurrence record tells us about how faults work. GSA *T*oday, 14(9), 4-10.

Weertman, J. (1964), Continuum distribution of dislocations on faults with finite friction. *Bull. Seismol. Soc. Am.*, *54*(4), 1035-1058.

Wills, C. J., II, R. W., and Bryant, W. A. (2007), California Fault Parameters for the National Seismic Hazard Maps and Working Group on California Earthquake Probabilities. *US Geological Survey Open File Report*.

Chapter 2: Building earthquake recurrence cycles using paleo-event chronologies of the San Andreas Fault System over the last 2000 years

2.1 INTRODUCTION

To determine temporal patterns in earthquake recurrence along a fault, a complete and thorough earthquake record is crucial. Modern instrumentation has provided a record of events for the past century, however geologists and seismologists depend on paleoseismic data to lengthen the record of large earthquakes back in time along different sections of the SAFS. These data strongly depend on field investigation methods to provide spatial and temporal information of a fault over several earthquake cycles.

2.2 HISTORIC AND PRE-HISTORIC EARTHQUAKES OF THE SAFS

Present-day seismic activity along the SAFS and across California is constantly monitored by modern geophysical instruments. Since the early 1900's, great advances is seismology were made possible due to the development of very sensitive seismographs and timing systems that allowed scientists to accurately locate earthquakes and model their source characteritics [*Havskov et al.,* 2010]. Before the development and availability of this technology, however; any deformation that occurred in California is highly uncertain and typically classified as historic or pre-historic. Historic earthquakes are those based on written records, missionary documents and photographic evidence from the last two centuries, as well as those recorded by modern instruments used before the digital era (1960's). Pre-historic earthquakes are those derived from paleoseismic investigations as described in Section 1.3 [i.e., *Grant et al.,* 2004; *Weldon et al.,* 2004].

The SAFS has produced many significant earthquakes that have been recorded over the last ~200 years. Figure 2.1 shows historical ruptures and dates of M_w>7 events along the entire SAFS from 1800 to 2004 [*Smith and Sandwell*, 2006]. Over 35 significant earthquakes have ruptured the SAFS over the

last two centuries. Four M_w>7.0 earthquakes between 1812 and 1906 ruptured two major sections spanning one or more segments of the fault system. The 1812 and 1857 events that ruptured the central section of the fault are believed to have overlapped. Likewise, the great 1906 earthquake overlapped the 1838 event in the northern section of the SAFS [*Ellsworth,* 1990].

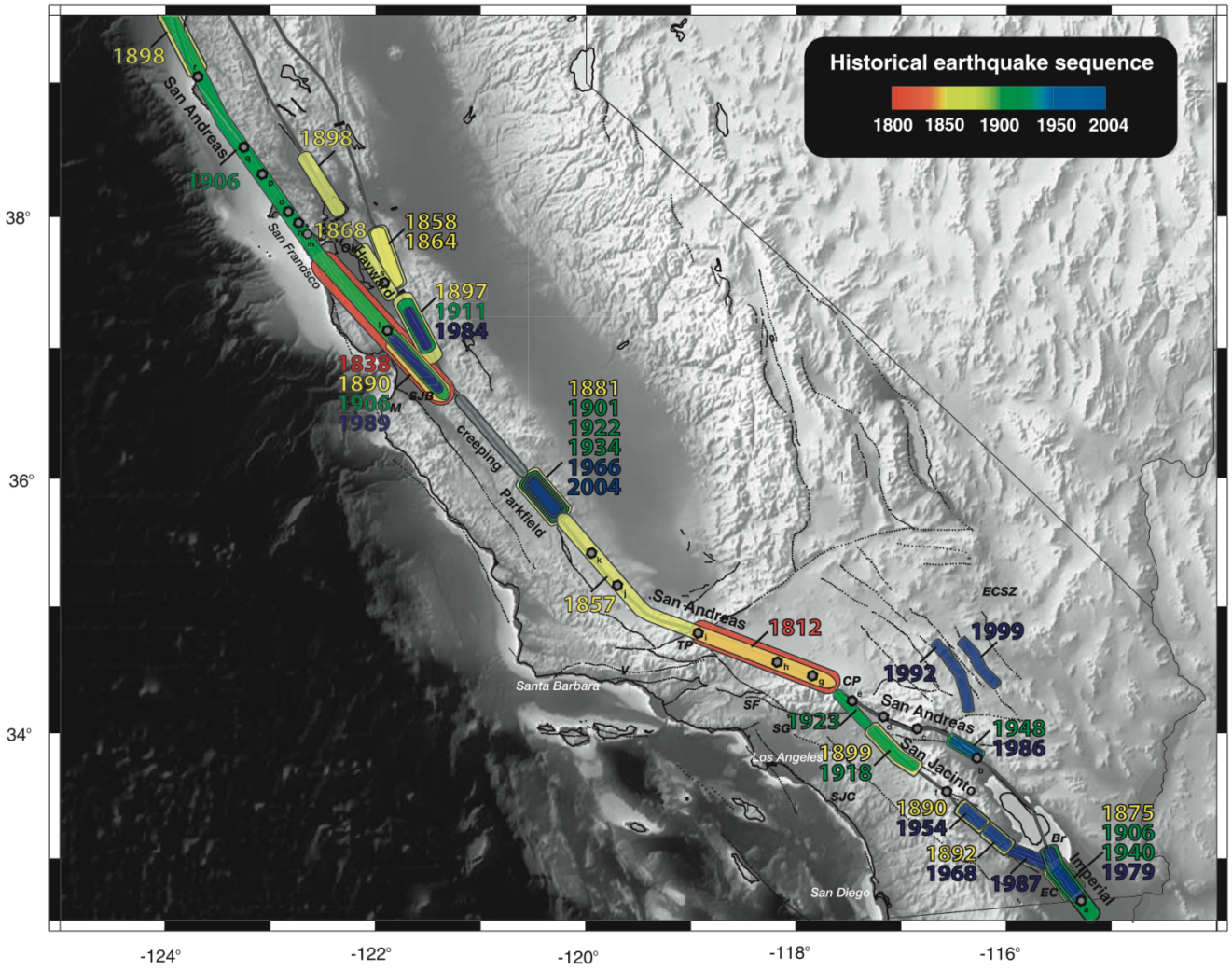

Figure 2.1. From *Smith and Sandwell* [2006]. Modeled historical earthquake ruptures (M.> 6.0) of the San Andreas Fault System from 1800 to 2004 [*Jennings*, 1994; *Toppozada et al*., 2002]. Colors depict era of earthquake activity from 1800 to 1850 (red), 1850 to 1900 (yellow), 1900 to 1950 (green), and 1950 to 2004 (blue). a, Imperial Fault; b, Thousand Palms; c, Burrow Flats; d, Plunge Creek; e, Pitman Canyon; f, Hog Lake; g, Wrightwood; h, Pallet Creek; i, Frazier Mountain; j, Bidart Fan; k, Las Yeguas; l, Grizzly Flat; m, Bolinas Lagoon; n, Dogtown; o, Olema; p, Bodego Harbor; q, Fort Ross; r, Point Arena; and s, Tyson's Lagoon. Labeled fault segments referred to in the text include the Imperial, San Andreas, San Jacinto, Parkfield, creeping section, and Hayward. Other locations include EC, El Centro; Br, Brawley; SJC, San Juan Capistrano; CP, Cajon Pass; SG, San Gabriel; SF, San Fernando; TP, Tejon Pass; V, Ventura; M, Monterey; SJB, San Juan Bautista; and Ok, Oakland.

Over the last 40 years, a large collaborative effort has also been made by the paleoseismic community to generate a rupture history for faults that comprise the San Andreas [i.e., *Petersen et al*., 1994; *Grant et al*., 1994; *Weldon et al*., 2004; *McGill et al*., 2008; *Toke et al*., 2009], Imperial [i.e., *Meltzner et al*., 2004], San Jacinto [i.e., *Fumal et al*., 2008; *Rockwell*, 2006] and Elsinore faults [i.e., *Vaughan et al*., 1999; *Dawson et al*., 2008]. *Smith and Sandwell* [2006] attempted to compile the results of these studies (up to 2004) into a simplified listing of major events (M>6.0) of the SAFS to be used in their initial stress evolution model (Figure 2.1, Table 2.1). Since then, various groups have published additional paleoseismic data that required a significant revision to the earthquake database utilized by *Smith and Sandwell* [2006]. The work described in the following sections addresses our approach to improve upon these results.

Table2.1. Prehistorical San Andreas Fault System Earthquakes From 1000 A.D. Based on Paleoseismic Trench Excavations. Modified from *Smith and Sandwell* (2006).

	Trench Site	Reference	Dates A.D.
a	Imperial Fault	Thomas and Rockwell [1996] and Sharp [1980]	~1670
b	Thousand Palms	Fumal et al. [2002b]	840–1150; 1170–1290; 1450–1555; >1520–1680
c	Burrow Flats	Yule [2000]	780–1130; 1120–1350; 1450–1600
d	Plunge Creek	McGill et al. [2002]	1450; 1630; 1690
e	Pitman Canyon	McGill et al. [2002]	~1450
f	Hog Lake	Rockwell et al. [2003]	1020; 1230; 1290; 1360; 1630; 1760
g	Wrightwood	Fumal et al. [2002a] and Biasi et al. [2002]	1047–1181; 1191–1305; 1448–1578; 1508–1569; 1647–1717
h	Pallet Creek	Biasi et al. [2002]	1031–1096; 1046–1113; 1343–1370; 1496–1599
i	Frazier Mountain	Lindvall et al. [2002]	1460–1600
j	Bidart Fan	Grant and Sieh [1994]	1218–1276; 1277–1510; 1405–1510
k	Las Yeguas (LY4)	Young et al. [2002]	1030–1460
l	Grizzly Flat	Schwartz et al. [1998] and Heingartner [1998]	1020–1610; 1430–1670
m	Bolinas Lagoon	Knudsen et al. [2002]	1050–1450
n	Dogtown	Cotton et al. [1982]	1100–1330; 1520–1690
o	Olema	Niemi and Hall [1992] and Niemi [1992]	1300–1660; 1560–1660
p	Bodego Harbor	Knudsen et al. [2002]	900–1390; 1470–1850
q	Fort Ross	Noller et al. [1993] and Simpson et al.[1996]	560–950; 920–1290; 1170–1650
r	Point Arena	Prentice [1989] and Baldwin [1996]	680–1640; 1040–1640
s	Tyson's Lagoon	Lienkaemper et al.[2002]	1360–1580; 1530–1740; 1650–1790

[a]Letters a–s correspond to paleoseismic locations plotted in Figure 2 . 1. Trench site name, references, and calendar year event dates are also given.

2.3 BUILDING THE SAFS PALEOSEISMIC DATABASE V2

A significant effort was made to compile the most recent and relevant paleoseismic data through a literature search. As a result, the SAFS Paleoseismic Database V2 (SAFS PDV2) was assembled, documenting fault slip history of each active fault segment in southern California, as reported in the literature. An Excel spreadsheet (Table 2.2, an example for the Mojave segment) was created to organize and display this information. A complete version of the SAFS PDV2 is included in Appendix 2A as Tables 2.A.1-4. Major segments included in this database are Parkfield, Carrizo, Cholame, Mojave, San Bernardino, Coachella, Brawley, Imperial, and Cerro Prieto. As part of this compilation of paleoseismic data, the San Jacinto and Elsinore faults were also included.

The SAFS PDV2 is organized as follows:				
***Column one*:** Event dates. Event dates as reported by authors; some of these events do not have a specific date and are listed as a range of time in which each event might have occurred.	***Column two:*** Author. Authors and respective publication date.	***Column three:*** Title. Title of publication	***Column four:*** Slip rates. Range of slip rates for each segment, where available.	***Column five:*** Remarks. Special remarks for each study site.

Table 2.2: Example of the paleoseismic database showing data compiled for the Mojave segment.

Event dates	Author	Title	Slip rate (mm/yr)	Remarks
534, 634, 697, 722, 781, 850, 1016, 1116, 1263, 1360, 1487, 1536, 1685, 1812, 1857	Weldon et al., 2004	Wrightwood and earthquake cycle: What a long recurrence record tells us about how faults work		
534, 634, 697, 722, 781, 850, 1016, 1116, 1263, 1360, 1487, 1536, 1685, 1812, 1857	Sharer et al., 2007	Paleoearthquakes on the Southern San Andreas Fault, Wrightwood, California, 3000 to 1500 B.C.: A new model fro evaluating paleoseismic evidence and earthquake horizons.		
1857, 1812, 1465-1695, 1329-1363, 1035-1165, 1015-1081, 981-1013, 775-919, 721-747, 658-684	Petersen et al., 1994	Fault slip rates and earthquake histories for active Fault in Southern California.	35.2-35.8	Pallet Creek
614-666, 749-775, 803-868, 914-986, 1031-1096, 1046-1113, 1343-1370, 1496-1599, 1812, 1857	Grant et al., 2002	Introduction to the special issue on paleoseismology of the San Andreas fault system.		Pallet Creek
533, 634, 697, 722, 781, 850, 1016, 1116, 1264, 1360, 1487, 1536, 1685, 1812, 1857	Biasi et al., 2009	San Andreas Fault rupture scenarios from multiple paleoseismic records: "stringing pearls"	n/a	Wrightwood
1812, 1857	Weldon et al., 2008	Appendix E: overview of the southern San Andreas Fault model	32 - 38	North segment
1812, 1857	Weldon et al., 2008	Appendix E: overview of the southern San Andreas Fault model	28.7	South segment
407-628, 551-681, 657-722, 695-740, 736-811, 800-881, 957-1056, 1047-1181, 1191-1305, 1448-1518, 1508-1569, 1647-1717, 1812, 1857	Fumal et al, Biasi et al and Weldon et al in Grant et al., 2002	Introduction to the special issue on paleoseismology of the San Andreas fault system.	20-40	Wrightwood
533, 634, 697, 722, 781, 850, 1016, 1116, 1264, 1360, 1487, 1536, 1685, 1812, 1857	Dawson et al., 2008	Appendix B: recurrence interval and event age data for type A Fault	6±2	Wrightwood
n/a	Petersen et al., 1994	Fault slip rates and earthquake histories for active Fault in Southern California.	48	Three Points
645, 764, 842, 956, 1067, 1084, 1360, 1547, 1812, 1857	Biasi et al., 2009	San Andreas Fault rupture scenarios from multiple paleoseismic records: "stringing pearls"	n/a	
690, 740, 800, 1000,1050, 1300, 1370, 1500, 1812, 1857	Yeats et al., 1990	Paleoseismicity: extending the record of earthquakes into prehistoric time	n/a	Dates are averages of the ranges shown on figure 1.
1856	Bennet et al., 1996	Global positioning system constraints on fault slip rates in southern California and northern Baja, Mexico	35±2	Locking depth 12km
1857	Johnson et al., 2007	Influence of lithosphere viscosity structure on estimates of fault slip rate in the Mojave region of the San Andreas Fault	25-35	14 events in the last 1600 years.
533, 634, 697, 722, 781, 850, 1016, 1116, 1264, 1360, 1487, 1536, 1685, 1812, 1857	Smith et al., 2006	Fault A model of the earthquake cycle along the San Andreas Fault System for the last 1000 years	40	
n/a	Weldon et al., 2009	Slip rate on the San Andreas Fault near little rock, CA.	20-40	

The SAFS PDV2 provides us with an efficient approach for evaluating the range of paleoseismic data available for each fault segment of the SAFS. From this entire compilation of data (Appendix 2A), it is clear that not all fault segments have equal amounts of paleoseismic data, as some fault segments have been studied more than others (i.e., Mojave, Parkfield, Imperial). Other complications have been noted, including the observation that several papers report significant variations in slip rates for the same fault segment (i.e., Parkfield segment, slip rate of 24.5±12/-7 mm/yr [*Toke et al*., 2009.] vs. 34±5 mm/yr [*Grant et al*., 2004]). Furthermore, the studied earthquake history for each segment is not the same; some segments have a history that extends over 2000 years or more (Carrizo, Mojave, Coachella), while others cover only a few hundred years (Parkfield, Imperial).

Some paleoseismic events are also published with a range of dates, which means that the dating techniques used by the author for the different samples yielded dates that were not exact and the author determined what would be a correct range of years for a certain event [*Grant et al*., 1994]. Furthermore, some of the published data conflicts with other studies (for example, *Grant et al.,* [2002] report an event dated at of 657-722 on the Mojave segment, while *Petersen et al*. [1994] report a range of 658-684). Such inconsistency may be due to the fact that earthquakes smaller than M5 do not leave many recognizable physical features but may alter or erase the evidence left behind from stronger earthquakes. Thus these paleoseismic records depend on the interpretation of each researcher [*McCalpin*, 1996].

2.4 Results and Discussion: Paleoseismic Earthquake Rupture Map

To better illustrate the results of Tables 2.1 and 2.A1-4 of the SAFS PDV2, a map of the SAFS paleoseismic history was constructed. Figure 2.2 shows an average of paleoseismic event dates from the most complete sets of data for each segment of the SAFS. As illustrated by Figure 2.2, there are several segments that reveal an extensive earthquake history.

Overall, the list paleo-earthquakes utilized by Smith and Sandwell [2006] (Table 2.1) has been significantly updated. For the Imperial segment there was a single event listed at ~1600 A.D. The new SAFS PDV2 lists events at 1525, 1575, 1650, 1700, 1949 and 1979 [Meltzner et al, 2006]. Burro Flats, Plunge Creek and Pittman Canyon paleoseismic sites (Figure 2.1, c, d, e) were included for the San Bernardino segment and the number of events increased from 3 within a range of time at Burro Flats to 7 (774, 1107, 1347, 1475, 1500, 1684, and 1812). For the Plunge Creek site, the number of events increased from 3 (1450, 1630, 1690) to 5 (1450, 1499, 1510-1730, 1619, 1812)[Dawson et al, 2002]. The Pittman Canyon site includes events at 931, 1173, 1313, 1437, 1704, and 1812 [Dawson et al, 2008]. The Hog Lake site along the Anza segment had 6 events previously listed and the new SAFS PDV2 has 10 events listed as range of possible occurrence (25-160, 160-305, 375-555, 995-110, 1075-1205, 1260-1325, 1285-1380, 1305-1400, 1530-1630, 1775-1805). A few of the events from the Smith and Sandwell [2006] table could possibly be included within the individual ranges from the new SAFS PDV2.

2.5 CONCLUSIONS

While our SAFS PDV2 is a reflection of the present-day paleoseismic record of the southern SAFS as reported in the literature, we note that maintaining such a database will continue to be a work in progress. There are still many gaps that need to be addressed in order to provide a better analysis of the earthquake history of California. Many of the paleoseismic sites have been studied for many years and will continue to be in the future, thus contributing even more data to aid in our interpretation and understanding of earthquake chronologies of the SAFS.

Figure 2.2 (next page). Paleoseismic earthquake map of southern San Andreas Fault System from the SAFS PDV2. Each color represents a different earthquake epoch, divided in 500 year spans and the length of the bars represent the approximate extent of the earthquake zone, but not the exact rupture length or magnitude. The information listed on for the Mojave segment reflects data from a common publication – Weldon 2004. Not all data listed in Table 2.2 appears in the map, only the dates used for Chapter 3.

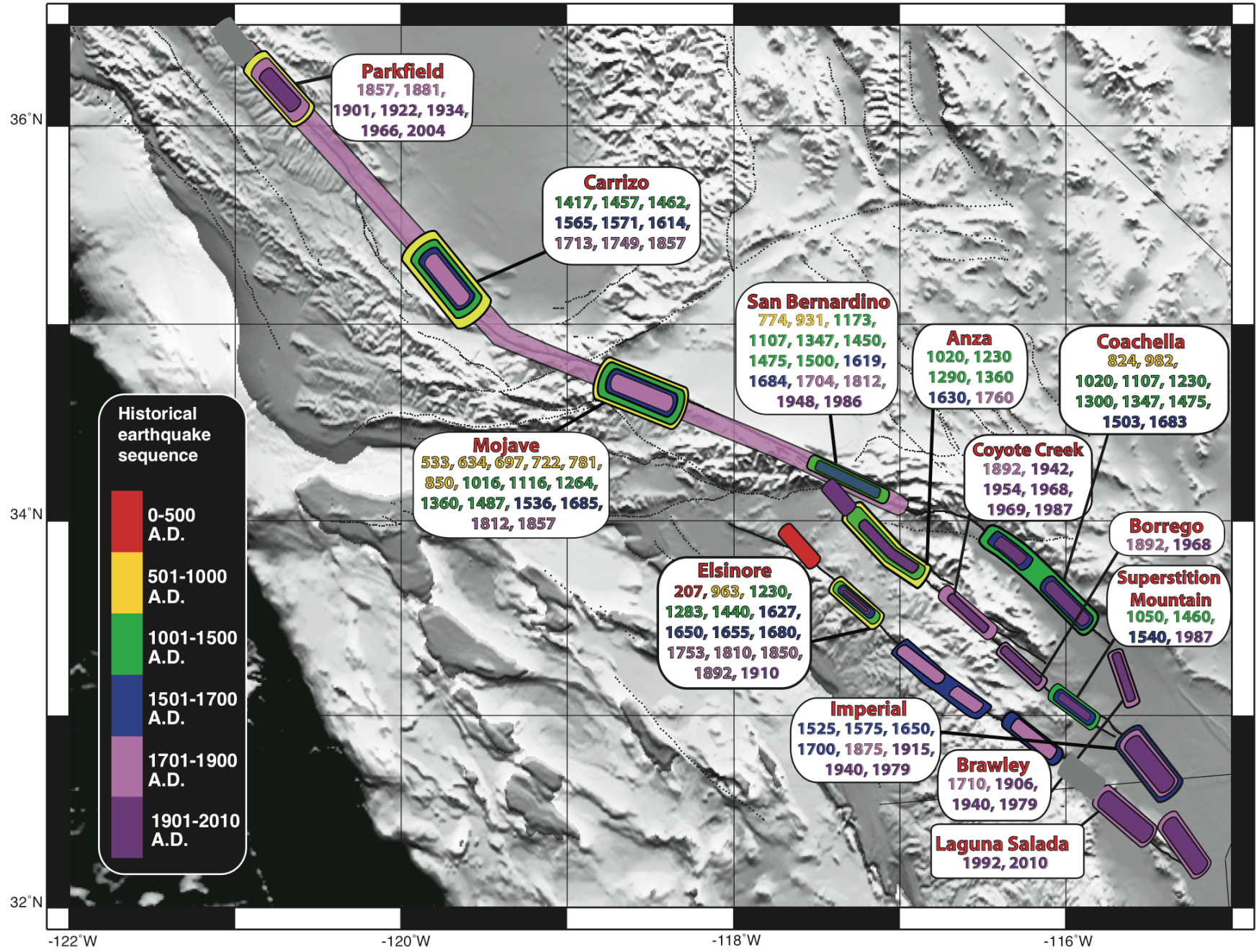
Parkfield
1857, 1881,
1901, 1922, 1934,
1966, 2004
Carrizo
1417, 1457, 1462,
1565, 1571, 1614,
1713, 1749, 1857
San Bernardino
774, 931, 1173,
1107, 1347, 1450,
1475, 1500, 1619,
1684, 1704, 1812,
1948, 1986
Anza
1020, 1230
1290, 1360
1630, 1760
Coachella
824, 982,
1020, 1107, 1230,
1300, 1347, 1475,
1503, 1683
Mojave
533, 634, 697, 722, 781,
850, 1016, 1116, 1264,
1360, 1487, 1536, 1685,
1812, 1857
Coyote Creek
1892, 1942,
1954, 1968,
1969, 1987
Borrego
1892, 1968
Elsinore
207, 963, 1230,
1283, 1440, 1627,
1650, 1655, 1680,
1753, 1810, 1850,
1892, 1910
Superstition
Mountain
1050, 1460,
1540, 1987
Imperial
1525, 1575, 1650,
1700, 1875, 1915,
1940, 1979
Brawley
1710, 1906,
1940, 1979
Laguna Salada
1992, 2010
Historical
earthquake
sequence
0-500
A.D.
501-1000
A.D.
1001-1500
A.D.
1501-1700
A.D.
1701-1900
A.D.
1901-2010
A.D.
36˚N
34˚N
32˚N
-122˚W
-120˚W
-118˚W
-116˚W

2.5 REFERENCES

Akciz, S. O., Ludwig, L. G., & Arrowsmith, J. R. (2009), Revised dates of large earthquakes along the Carrizo section of the San Andreas Fault, California, since AD 1310±30. *J. Geophys. Res.*, 114(B1),B01313.

Anderson, J. G., and Bodin, P. (1987), Earthquake recurrence models and historical seismicity in the Mexicali-Imperial Valley. *Bull. Seismol. Soc. Am.*,77(2), 562-578.

Behr, W. M., Rood, D. H., Fletcher, K. E., Guzman, N., Finkel, R., Hanks, T. C., and Yule, J. D. (2010), Uncertainties in slip-rate estimates for the Mission Creek strand of the southern San Andreas fault at Biskra Palms Oasis, southern California. *Geological Society of America Bulletin*, 122(9-10), 1360-1377.

Bennett, R. A., Rodi, W., & Reilinger, R. E. (1996), Global Positioning System constraints on fault slip rates in southern California and northern Baja, Mexico. *J. Geophys. Res.*, 101(B10), 21943-21.

Bent, A. L., and Helmberger, D. V. (1991), A re-examination of historic earthquakes in the San Jacinto fault zone, California. *Bull. Seismol. Soc. Am.*, 81(6), 2289-2309.

Biasi, G. P., and Weldon, R. J. (2009), San Andreas fault rupture scenarios from multiple paleoseismic records: Stringing pearls. *Bull. Seismol. Soc. Am.,* 99(2A), 471-498.

Brothers, D. S., Driscoll, N. W., Kent, G. M., Harding, A. J., Babcock, J. M., and Baskin, R. L. (2009), Tectonic evolution of the Salton Sea inferred from seismic reflection data. *Nature Geoscience*, 2(8), 581-584.

Dawson, T., Rockwell, T., Weldon II, R. J., and Wills, C. (2007), Summary of geologic data and development of a priori rupture models for the Elsinore, San Jacinto and Garlock faults; Appendix F in The Uniform California Earthquake Rupture Forecast, version 2 (UCERF 2). US Geol. Surv. Open-File Rept. 2007-1437-F.

Doser, D. I. (1992), Historic earthquakes (1918 to 1923) and an assessment of source parameters along the San Jacinto fault system. *Bull. Seismol. Soc. Am.*, 82(4), 1786-1801.

Dawson, T. E., Weldon II, R. J., and Biasi, G. P. (2007), Appendix B: Recurrence interval and event age data for type A faults. US Geol. Surv. Open-File Rept, 2007-1437.

Ellsworth, W. L. (1990), The San Andreas fault system, California. *US Geol. Surv. Prof. Pap*, *1515*, 153-185.

Fumal, T. E. Dawson, T. E., Flowers, R., Hamilton, J. C., Heingartner, G. F., Kessler, J., and Samrad, L. (2004), Photomosaics and logs of trenches on the San Andreas fault at Mill Canyon near Watsonville, California. US Geological Survey.

Grant, L.B. and K. Sieh (1994), Paleoseismic evidence of clustered earthquakes on the San Andreas fault in the Carrizo plain, California. *J. Geophys. Res.*, 99, 6819-6841.

Grant, L. B., and Lettis, W. R. (2002), Introduction to the special issue on paleoseismology of the San Andreas fault system. *Bull. Seismol. Soc. Am.*, 92(7), 2551-2554.

Grant, L.B. and M.M. Gould (2004), Assimilation of paleoseismic data for earthquake simulation. *Pure and Applied Geophysics,* 161, 2295-2306.

Harden, J. W., and Matti, J. C. (1989), Holocene and late Pleistocene slip rates on the San Andreas fault in Yucaipa, California, using displaced alluvial-fan deposits and soil chronology. *Geological Society of America Bulletin*,101(9), 1107-1117.

Janecke, S. U. (2011), High Geologic Slip Rates Since Early Pleistocene Initiation of the San Jacinto and San Felipe Fault Zones in the San Andreas Fault System, Southern California, USA (Vol. 475). *Geological Society of America Bulletin*.

Johnson, K. M., Hilley, G. E., and Bürgmann, R. (2007), Influence of lithosphere viscosity structure on estimates of fault slip rate in the Mojave region of the San Andreas fault system. *J. Geophys. Res.*, 112(B7), B07408.

Kendrick, K. J., Morton, D. M., Wells, S. G., and Simpson, R. W. (2002), Spatial and temporal deformation along the northern San Jacinto fault, southern California: implications for slip rates. *Bull. Seismol. Soc. Am.*, 92(7), 2782-2802.

McCalpin, J. P. Paleoseismology. Academic Press, San Diego, 1996.

McGill, S., Weldon, R. J., and Owen, L. (2008), Preliminary slip rates along the San Bernardino strand of the San Andreas fault.

Meltzner, A. J., Rockwell, T. K., and Owen, L. A. (2006), Recent and Long-Term Behavior of the Brawley Fault Zone, Imperial Valley, California: An Escalation in Slip Rate?. *Bull. Seismol. Soc. Am.*, 96(6), 2304-2328.

Petersen, M. D., and Wesnousky, S. G. (1994), Fault slip rates and earthquake histories for active faults in southern California. *Bull. Seismol. Soc. Am.*, 84(5), 1608-1649.

Rockwell, T., Seitz, G., Dawson, T., and Young, J. (2006), The long record of San Jacinto fault paleoearthquakes at Hog Lake: Implications for regional patterns of strain release in the southern San Andreas fault system. *Seismological Research Letters*, 77(2), 270.

Rust, D. (2005), Palaeoseismology in steep terrain: the big bend of the San Andreas fault, Transverse Ranges, California. Tectonophysics, 408(1), 193-212.

Scharer, K. M., Weldon, R. J., Fumal, T. E., and Biasi, G. P. (2007), Paleoearthquakes on the southern San Andreas fault, Wrightwood, California, 3000 to 1500 BC: A new method for evaluating paleoseismic evidence and earthquake horizons. *Bull. Seismol. Soc. Am.*, 97(4), 1054-1093.

Sieh, K. E., and Jahns, R. H. (1984), Holocene activity of the San Andreas fault at Wallace creek, California. *Geological Society of America Bulletin*, 95(8), 883-896.

Smith, B.R. and D.T. Sandwell (2006), A model of the earthquake cycle along the San Andreas Fault System for the past 1000 years, *J. Geophys. Res.*, 111, B01405, doi:10.1029/2005JB003703.

Toké, N.A. and JR. Arrowsmith (2006) "Reassessment of a slip budget along the Parkfield segment of the San Andreas Fault" *Bull. Seismol. Soc. Am.,* 96, 339-348.

Toké, N.A., JR. Arrowsmith, J.J. Young, C.J. Crosby (2006) "Paleoseismic and post-seismic observations of fault slip along the Parkfield segment of the San Andreas Fault." *Bull. Seismol. Soc. Am.,* 96, 221-238.

Toké, N. A., J.R. Arrowsmith, M.J. Rymer, A. Landgraf, J. Coyan, M. Busch, D . Haddad "Long-lived creep, M6 earthquakes, and a Holocene slip rate for the main trace of the San Andreas Fault at Parkfield, California" Annual Southern California Earthquake Center Meeting, Proceedings and Abstracts, vol. 19, Palm Springs, California, September 12-16th, 2009.

Van Der Woerd, J., Klinger, Y., Sieh, K., Tapponnier, P., Ryerson, F. J., and Mériaux, A. S. (2006). Long-term slip rate of the southern San Andreas fault from 10Be-26Al surface exposure dating of an offset alluvial fan. *J. Geophys. Res.*, 111(B4), B04407.

Vaughan, P. R., Thorup, K. M., and Rockwell, T. K. (1999). Paleoseismology of the Elsinore fault at Agua Tibia Mountain southern California. *Bull. Seismol. Soc. Am.*, 89(6), 1447-1457.

Weldon, R., Scharer, K., Fumal, T., and Biasi, G. (2004). Wrightwood and the earthquake cycle: What a long recurrence record tells us about how faults work. GSA today, 14(9), 4-10.

Weldon, R. J., II, G., and Biasi, C. J. (2007). Wills, and TE Dawson (2007). Overview of the southern San Andreas fault model; Appendix E in The Uniform California Earthquake Rupture Forecast, version 2 (UCERF 2). US Geol. Surv. Open-File Rept. 2007-1437-E.

Yeats, R. S., and Schwartz, P. D. (1990). Paleoseismicity: extending the record of earthquakes into prehistoric time. Episodes, 13 (1), 9, 12.

Chapter 3: Estimating variations in locking depth for the Mojave segment of the San Andreas fault over the past 1500 years from paleoseismic stress drop

(to be submitted to the *Journal of Geophysical Research*, Summer 2013)

3.1 ABSTRACT

The recurrence and slip of earthquakes along active fault systems such as the San Andreas Fault System (SAFS), to first order, should depend largely on the stress that accumulates between slip events and the release mechanism, or stress drop, of a fault segment. This model, however, often fails to explain the large differences in earthquake recurrence intervals and slip for published paleoseismic datasets. To better understand how stress accumulation can vary over multiple earthquake cycles, we investigate the role of paleoseismic fault locking depth of the Mojave segment of the SAFS. We use published date and slip estimates spanning the last 1500 years [*Weldon et al*., 2004] and a 4-D earthquake stress model [*Smith-Konter and Sandwell*, 2009] to tune model-derived stress drops for each earthquake cycle to fit stress drop estimates derived from paleoseismic data. For each earthquake cycle, we assume a constant slip rate and systematically adjust the locking depth of the Mojave segment to best match the paleoseismic data. For 9 of the 14 events studied, we find that model-derived stress drops can accurately predict paleoseismic stress drop, given the range of tested fault depths (5-25 km), when slip uncertainties are accounted for. We also identify a positive correlation between event locking depth and stress drop, where low stress drop events are best modeled with a larger fault depth and higher stress drop events are best modeled with a moderate fault depth. In terms of the paleoseismic data, this relationship suggests that when stress is stored by a fault that is more deeply locked, stress will accumulate at a slower rate throughout an earthquake cycle, producing an overall lower stress drop than would be expected for a shallow fault. From these results, we propose that realistic variations in locking depth spanning 9 of the 14 earthquake cycles of the Mojave segment could have generated enough variation in earthquake cycle stress rate to support non-characteristic stress drop behavior.

3.2 INTRODUCTION

The San Andreas Fault System (SAFS) in California is considered the primary tectonic boundary between the North American and the Pacific plates (Figure 3.1). This transform margin developed approximately 29 Ma and accommodates 35-50 mm/yr of slip along its ~1500 km of length [*Atwater, et al.,* 1973]. The fault has ruptured in at least 70 major earthquakes (M_w>6.0) over the past 1500 years (ref). Despite the large amounts of data generated from one of the most thoroughly studied faults on the planet, there are still many unanswered questions regarding segmentation, rupture patterns, and characteristics of large earthquakes along the SAFS. Moreover, standard earthquake cycle theories often fail to explain the large differences in earthquake recurrence intervals and slip from published paleoseismic datasets: why do events sometimes rupture on the order of 10s of years, and other times require 100s of years to accumulate substantial stress before failing in a large earthquake?

The recurrence of the largest earthquakes along an active fault system such as the SAFS, to first order, should depend largely on the stress that accumulates between slip events and the release mechanism, or stress drop, of a fault segment. Stress accumulation rate (Figure 3.1) will vary as a function of fault slip rate, fault depth, fault orientation, and several other rheological parameters. Furthermore, fault segments with relatively high stress accumulation rates (i.e., the Imperial segment) are more likely to have shorter average recurrence intervals (~40 years for Imperial), while segments with lower stress accumulation rates (i.e., the Mojave segment) have a longer average recurrence intervals (~150 years for Mojave) [*Smith and Sandwell*, 2003; *Smith-Konter and Sandwell*, 2009].

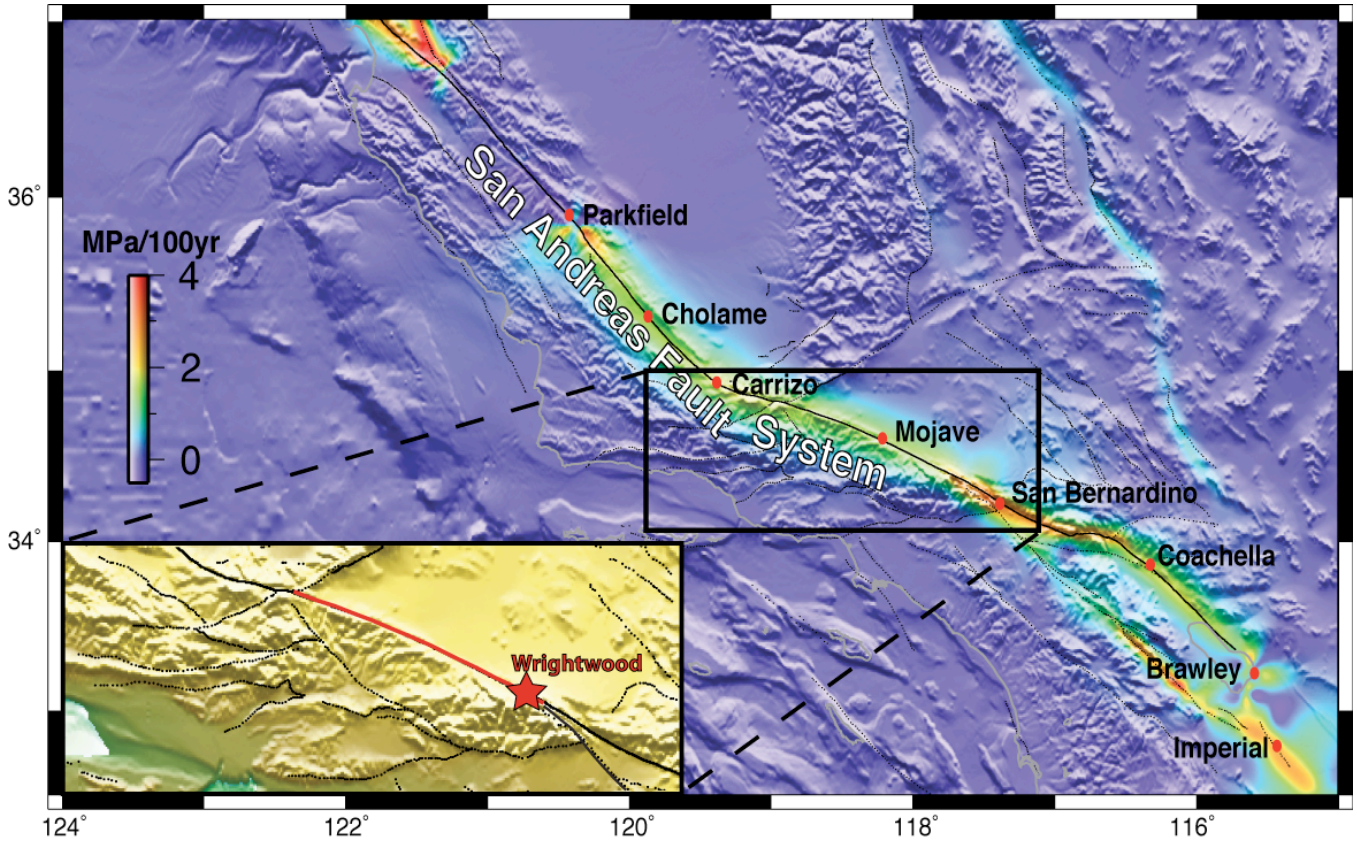

Figure 3.1. Stress accumulation rate model of the southern San Andreas Fault System [*Smith and Sandwell*, 2006; *Smith-Konter and Sandwell*, 2009]. The model primarily represents interseismic stress rates of primary fault segments using slip rates and locking depths constrained by the EarthScope PBO GPS velocity field. Inset shows regional map of the Mojave segment of the SAFS (red line), defined by previous geologic studies [i.e., *WGCEP*, 1995; 2007]. The red star represents the location of Wrightwood paleoseismic site.

Previous work suggests that the rate of stress accumulation is highly sensitive to fault locking depth, where shallowly locked faults accumulate stress at higher rates than deeply locked faults [*Smith-Konter and Sandwell*, 2009]. Thus, an accurate estimate of fault locking depth is a critical quantity for forecasting the magnitude of future earthquakes and also for assessing stress accumulation behavior throughout past earthquake cycles. When modeling seismic hazards, a common approach is to assume a common depth for all fault segments, however estimates from both geodesy and seismology suggest that effective fault locking depths (or seismogenic thicknesses) can vary spatially and temporally. For example, geodetically determined locking depths vary from 5.9 to 21.5 km for the southern SAFS, while seismically-determined depths range from 12.0 to 20.7 km [*Smith-Konter et al.*, 2011]. There is also

evidence to suggest that a fault locking depth may change throughout each earthquake cycle [*Meade and Hager, 2005*]. We extend these ideas to investigate the impact of stress accumulation rates and stress drop due to changes in locking depth spanning multiple earthquake cycles.

To effectively balance seismic moment accumulation and release rates, an earthquake record long enough to reflect characteristic fault system activity is needed [*Meade and Hager*, 2005]. There are several key locations along the SAFS where the earthquake record is long enough to study stress evolution over multiple earthquake cycles. The Mojave segment (Figure 3.1) is a well-studied section of the SAFS [i.e., *Sieh et al*., 1989; *Fumal et al*., 1993; *Weldon et al*., 2004; *Scharer et al*., 2007, 2010] and an ideal target because of the completeness of the paleoseismicpaleoseimic record and the accessibility to surface displacement per event data. The Mojave segment has also been extensively studied geodetically, with a geodetically-determined slip rate of 28 ± 7 mm/yr [*WGCEP,* 2007] and an effective locking depth of 16.8 ± 0.4 km [*Smith-Konter et al.,* 2011]). Based on these fault characteristics, the Mojave segment is estimated to presently accumulate stress at a rate of 1.29 MPa/100 years [*Smith-Konter and Sandwell*, 2009], although this rate may have varied over the multiple earthquake cycles.

In this study, we investigate variations in stress due to changes in paleoseismic locking depth spanning multiple earthquake cycles of the Mojave segment of the SAFS. Specifically, we investigate the relevance of variable locking depth through time and how this may have caused significant changes in earthquake cycle stress accumulation, coseismic stress drop, and paleoseismic slip. Using a 4-D earthquake stress model, we tune model-derived stress drops for each earthquake cycle to fit stress drop estimates derived from paleoseismic offset data spanning the last 1500 years. Best-fitting model locking depths, ranging from 5-25 km, are evaluated for 14 Mojave segment earthquake cycles. Here we demonstrate how these variations in fault depth may have modified the dimensions of the fault zone over the past 1500 years, and thus significantly altered the rate of stress accumulation between earthquakes to produce non-characteristic slip quantities.

3.3 PALEOSEISMIC DATA

The Wrightwood paleoseismic site (34º22'11" N; -117º40'04" W)[*Scharer et al.,* 2007], located at the southern edge of the Mojave segment (Figure 3.1), consists of 45 paleoseismic trenches that have been thoroughly studied for over 25 years [*Weldon et al.,* 2004]. The Wrightwood site is defined as a structural depression created by the SAF that has been intermittently inundated by debris flows that were deposited into the linear valley that follows the fault [*Weldon et al*., 2002; 2004]. These layers of debris provided the opportunity to unravel the timing for several sequences of events. Data from the Wrightwood site (Table 3.1) provide critical information about the recurrence behavior of large earthquakes, specifically paleoseismic event dates, mean time intervals between events, slip amount (offset), and related uncertainties associated with each event. Based on these data, the mean recurrence interval for the 15 Wrightwood events is 105 yrs (31-165 yrs per event) and the mean slip is 3.2 m (0.7-7 m per event). Because of the nature of paleoseismic dating methods, uncertainties in dates and offsets range from 21 to 158 years and 0.5 m to 9.9 m for events that occurred on the Mojave segment.

For this study, we make the simplifying assumption that these data are applicable to the entire extent of the Mojave segment; however *Weldon et al*. [2004] cautiously note that these displacements are only reflective of earthquake activity at the Wrightwood site and do not necessarily represent the displacement of the entire segment. As an actual earthquake slip decreases as it approaches the limit of the rupture, the displacements at this site might be small earthquakes or tail ends of larger events as in 1857 [*Weldon et al*., 2004]. Neighboring paleoseismic sites (Pallet Creek and Pittman Canyon [*Scharer et al*., 2007], Figure 1.4) provide the opportunity to extrapolate data to cover a larger area of the segment, however we limit the data for this study to that from *Weldon et al*. [2004] for simplicity and consistency. There is significant evidence that the middle section of the Mojave segment ruptured during the 1812 and the 1857 events. All previous events dating back to 534 A.D. were identified at various points along the network of trenches at the site [*Weldon et al*., 2004; *Sharer et al.,* 2010].

Table 3.1. Paleoseismic data at Wrightwood, CA. Modified from *Weldon et al*. [2004].

Mean age (1σ range)	Recurrence interval (yr)	Offset $\overline{D}$ (m; 1σ range)
1857 (Historic)	44	1.0 (0.5-2.0)
1812 (Historic)	127	3.5 (1.0-7.0)
1685 (1662-1700)	149	3.5 (1.0-7.0)
1536 (1518-1542)	49	7.0 (3.0-9.0)
1487 (1463-1502)	127	0.7 (0.0-2.8)
1360 (1343-1370)	97	0.7 (0.0-2.8)
1263 (1230-1286)	147	3.7 (1.9-5.6)
1116 (1071-1152)	100	1.8 (1.1-3.4)
1016 (1071-1152)	166	1.5 (0.7-3.1)
850 (825-864)	69	6.6 (3.0-9.9)
781 (758-794)	59	5.2 (2.5-7.5)
722 (706-729)	25	3.0 (1.2-6.3)
697 (676-708)	63	4.1 (1.4-8.2)
634 (602-658)	100	1.8 (1.0-5.1)
534 (464-594)	-	1.9 (1.0-3.8)

3.4 4-D EARTHQUAKE CYCLE MODELING

Using a 4-D semi-analytic crustal deformation model [*Smith and Sandwell*, 2003; 2006; *Smith-Konter and Sandwell*, 2009], we simulate multiple earthquake cycles of interseismic stress accumulation, coseismic stress drop, and postseismic stress relaxation. To construct these models, we allow interseismic stress to accumulate at rates consistent with Figure 3.1, which assumes a constant geologic slip rate of 33 mm/yr [*Weldon et al*., 2002] for the Mojave segment. For our starting model, we adopt a constant locking depth of 15 km as an average between the seismic and the geodetic locking depth estimates [*Smith-Konter et al*., 2011]. We also make a simplifying assumption that complete stress release per earthquake cycle (i.e., all stress that has accumulated) occurs along the Mojave

segment at years indicated by the earthquake event dates from Table 3.1. Stress accumulation (and subsequent stress drop) is calculated for the entire earthquake history of the Mojave segment (Figures 3.2-3.3), beginning with a first event in year 634 and cycling forward to present day (the 534 event was excluded from our analysis because of its incomplete time interval). To illustrate the variations in stress accumulation prior to each event, Figure 3.2 shows model snapshots (in map view) acquired 1 year prior to each pre-historical earthquake. These snapshots approximate the total stress drop that is simulated for the Mojave segment immediately following each event. A time-series of stress accumulation and stress drop is provided in Figure 3.3. To first order, this model simulates a slip-predictable stress drop and earthquake offset pattern [*Scholz*, 1990, also see Figure 1.2], where a constant slip (or stress) rate throughout each earthquake cycle produces coseismic slip magnitudes (and stress drops) that are proportional to the recurrence time spanning each event. It is also important to note that 3-D and temporal effects (i.e., stress shadows due to postseismic stress relaxation (grey zones in Figure 3.3) [*Harris and Simpson,* 1996, 1998; *Harris,* 1998] also contribute to the overall stress field.

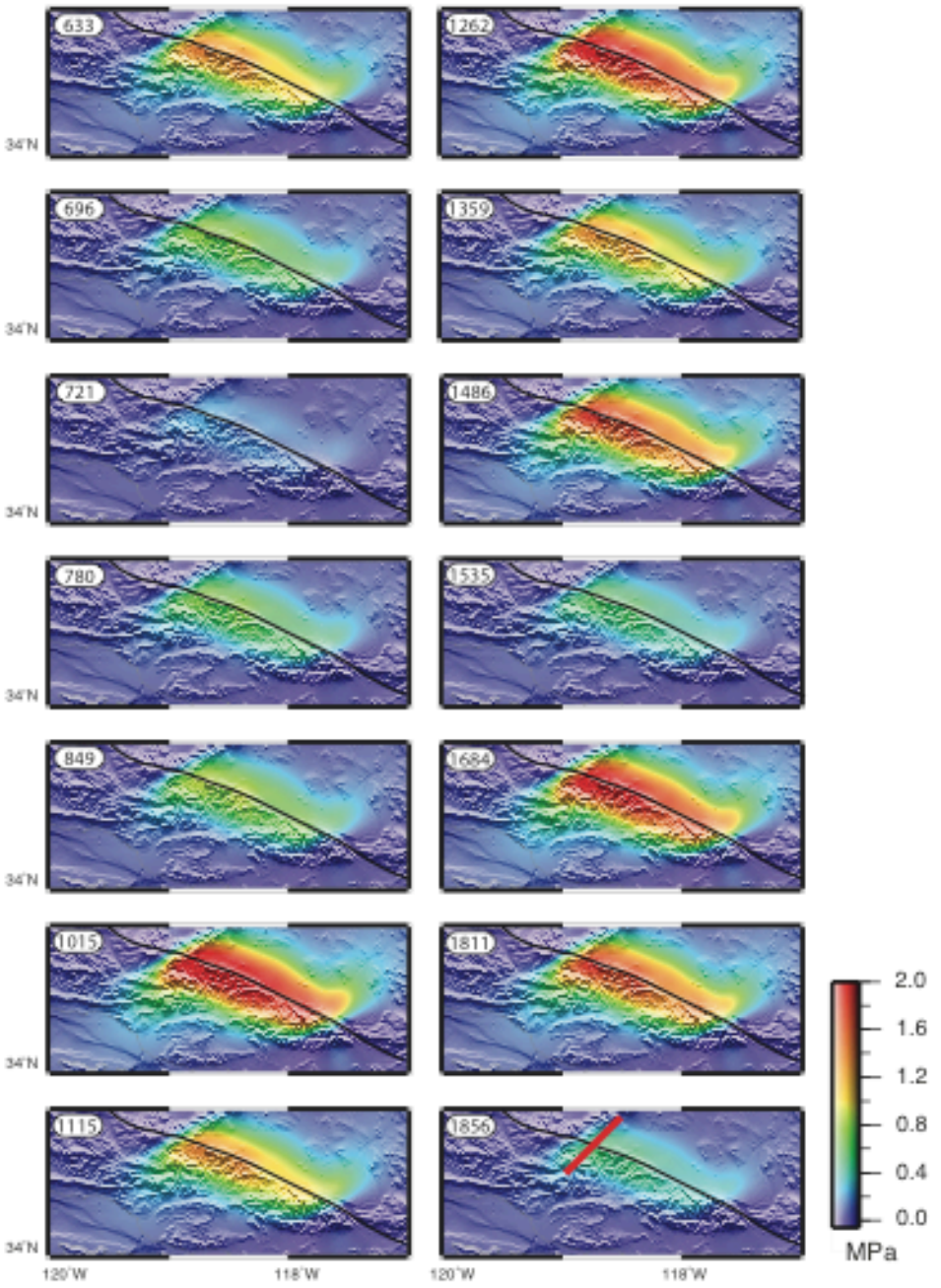

Figure 3.2. Snapshots of stress accumulation (approximating coseismic stress drop) for the Mojave segment, estimated using a fixed slip rate of 33 mm/yr and a locking depth of 15 km. Stress accumulation is shown for the year preceding each estimated earthquake event year (Table 3.1). Red line in the 1856 box represents the location where stress is sampled.

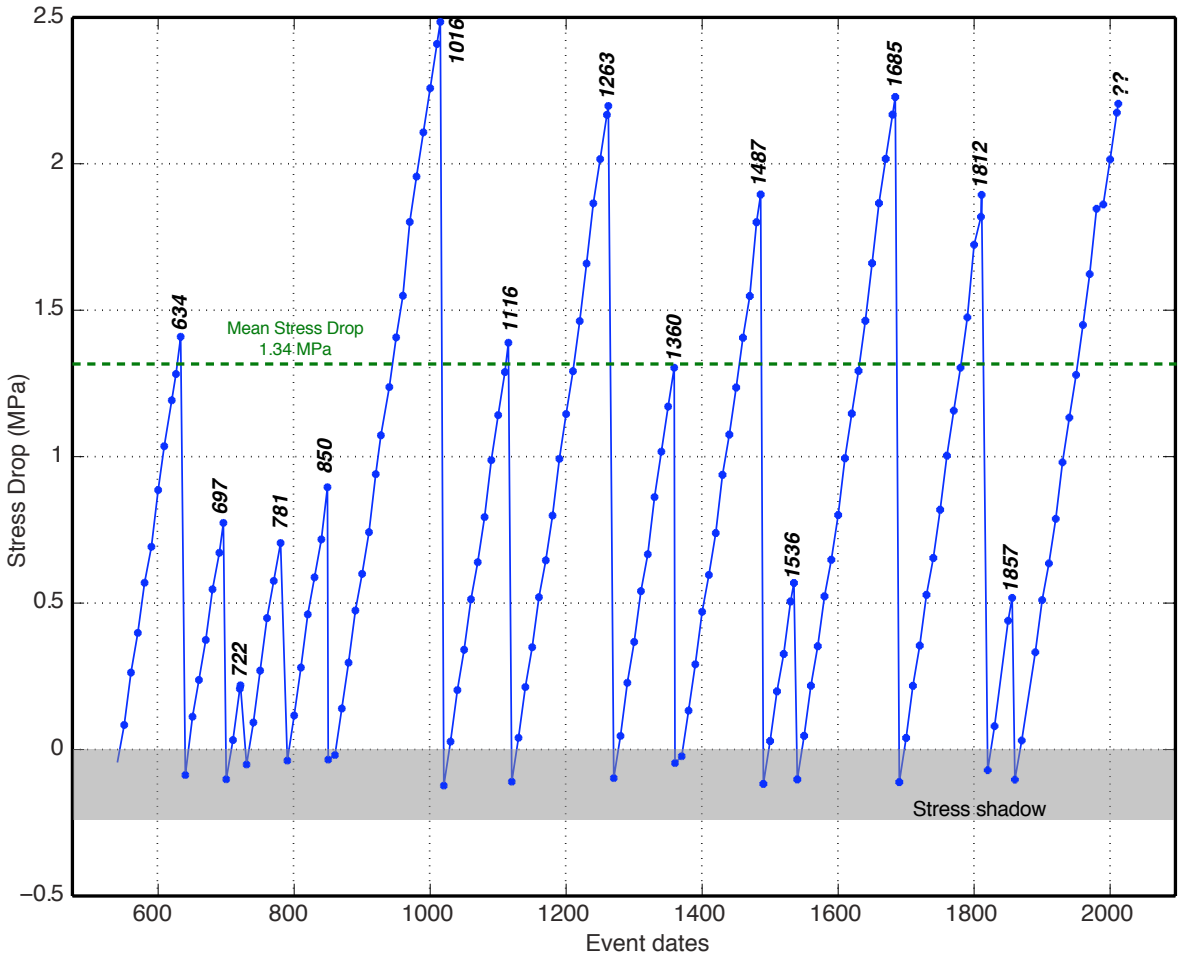

Figure 3.3. Time-series of model stress accumulation and stress drop. For this plot, stress values are obtained using 10 year sampling intervals?, supplemented by stress magnitudes obtained 1 year prior to each paleoseismic event, as in Figure 3.2. Peak stress drop magnitudes are estimated by extracting profiles of stress across a ~78 km fault-perpendicular transect (shown in the 1856 snapshot in Figure 3.2) at the northernmost point of the Mojave segment where stress is at a maximum. In this model, a fixed slip rate of 33 mm/yr and a locking depth of 15 km are assumed. The gray box represents stresses that fall below zero after each event (i.e., stress shadows) where stress relaxation occurs.

To construct earthquake cycle stress models such as these, an assumed earthquake slip history is prescribed based on paleoseismic evidence and thus the level of stress accumulation derived from the models is dependent on a comprehensive paleoseismic database (Table 3.1). Although the stress accumulation rate throughout each of these earthquake cycles is ~ 1.5 MPa/100yrs [*Smith-Konter and Sandwell,* 2009] (with small deviations within each earthquake cycle that account for postseismic relaxation), the amount of stress that accumulates prior to each event is directly proportional to the

earthquake recurrence interval: larger temporal spans between events permit larger amounts of stress to accumulate. For example, just before the 1016, 1263, and 1685 events, where the recurrence interval is over 140 years, stress accumulation (and implied stress drop) exceeds 2.0 MPa (Figures 3.2-3.3). Alternatively, events with shorter recurrence intervals like the 722, 781, 1536, and 1857 events yield a much smaller quantity of accumulated stress (< 0.75 MPa). These model-derived stress drops are then assembled for comparison with paleoseismic slip-derived stress drops (discussed in Section 3.5).

3.5 ESTIMATING STRESS DROP: PALEOSEISMIC DATA AND 4-D MODELS

Earthquake stress drop is a quantity that we can model and also empirically estimate using the ratio of the coseismic fault slip to an appropriate scale length (fault length, fault depth, or the entire fault area) [*Kanamori*, 1994] over which the slip occurred. A priori work (Appendix 3A) suggests that a fault area scale length (Equation 3.1) yields data-derived stress drop averages that are best reproduced by our 4-D model:

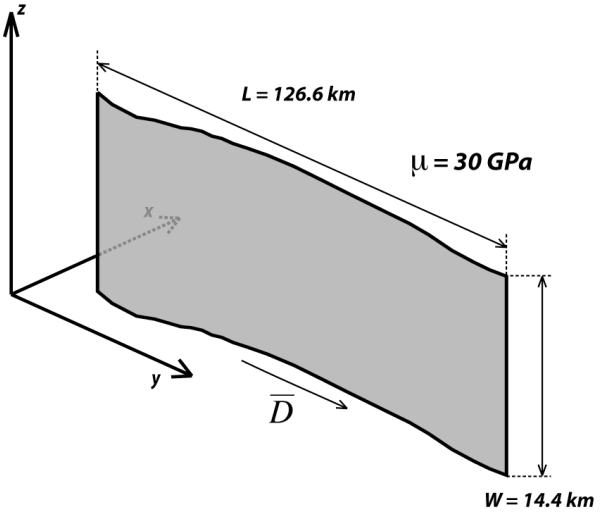

Figure. 3.4. Mojave segment fault dimensions used to calculate stress drop.

$$\Delta\sigma = \mu \frac{\overline{D}}{\sqrt{L \cdot W}} \quad \textbf{(3.1)}$$

where $\Delta\sigma$ represents stress drop, μ is the crustal shear modulus, L is the fault segment length, W is the fault depth, and $\overline{D}$ is paleoseismic slip (represented by the slip estimates in Table 3.1) (Figure 3.4). Paleoseismic slip-derived stress drop estimates, in this case assuming a constant fault depth of 15 km, are provided in Figure 3.5. These results suggest paleoseismic slip-derived stress drops along the Mojave segment that range from 0.49 to 4.92 MPa, with a mean stress drop of 2.21 MPa and standard deviation of 1.45 MPa.

Modelmodel stress drop is taken to be the peak stress accumulation magnitude just prior to each simulated earthquake event spanning all 14 earthquake cycles (Figure 3.3). Model-derived stress drops range from 0.24 to 2.54 MPa, with a mean stress drop of 1.34 MPa and standard deviation of 0.73 MPa. These values, spanning all 14 earthquake cycles, suggest that the mean paleoseismic slip-derived stress drop (2.21 MPa) is nearly double the stress drop estimated by our starting model, assuming a constant 15 km fault depth.

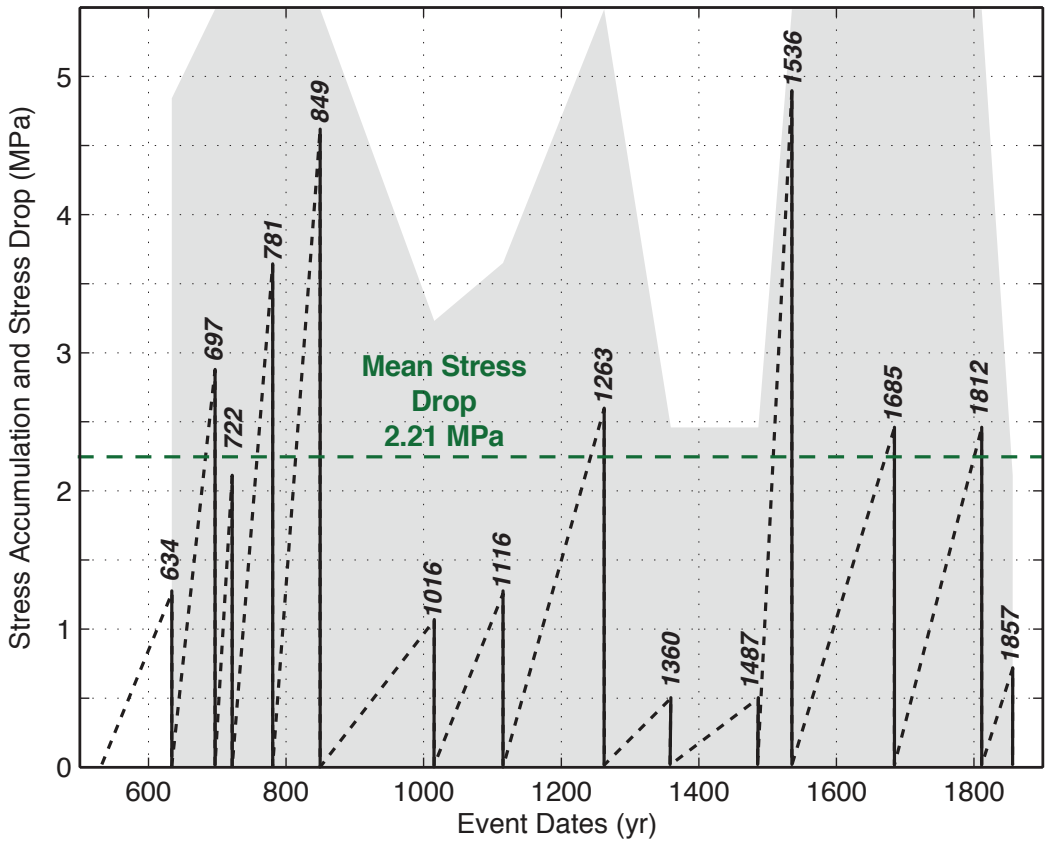

Figure 3.5. Paleoseismic stress drop and estimated stress accumulation. Stress drop (vertical drop) for each event is calculated from paleoseismic event slip magnitudes (Table 3.1), assuming a constant fault depth of 15 km. Dashed lines represent an ideal slope of stress accumulation, estimated by connecting a zero stress balance for each previous event to the calculated stress drop for each event. The gray background represents the uncertainty in stress drop based on the uncertainty in offsets given in Table 3,1.

Based on the paleoseismic data (Table 3.1), events with shorter recurrence intervals (i.e., years 697, 722, 781, 850, and 1536) are typically accompanied by higher slip events and thus higher stress drops, while longer recurrence intervals (i.e., years 1016, 1116, 1262, 1685, and 1812) are typically accompanied by lower stress drops (Figure 3.6a). From these data, high stress rates could be inferred for short recurrence intervals and low stress rates for longer recurrence intervals [*Weldon et al*., 2004]. Alternatively, our 4-D earthquake cycle model predicts just the opposite (Figure 3.6b), as it behaves according to a constant stress accumulation rate for all earthquake cycles. Thus short recurrence intervals are predicted to have smaller stress drops and longer intervals predicted to have larger stress drops.

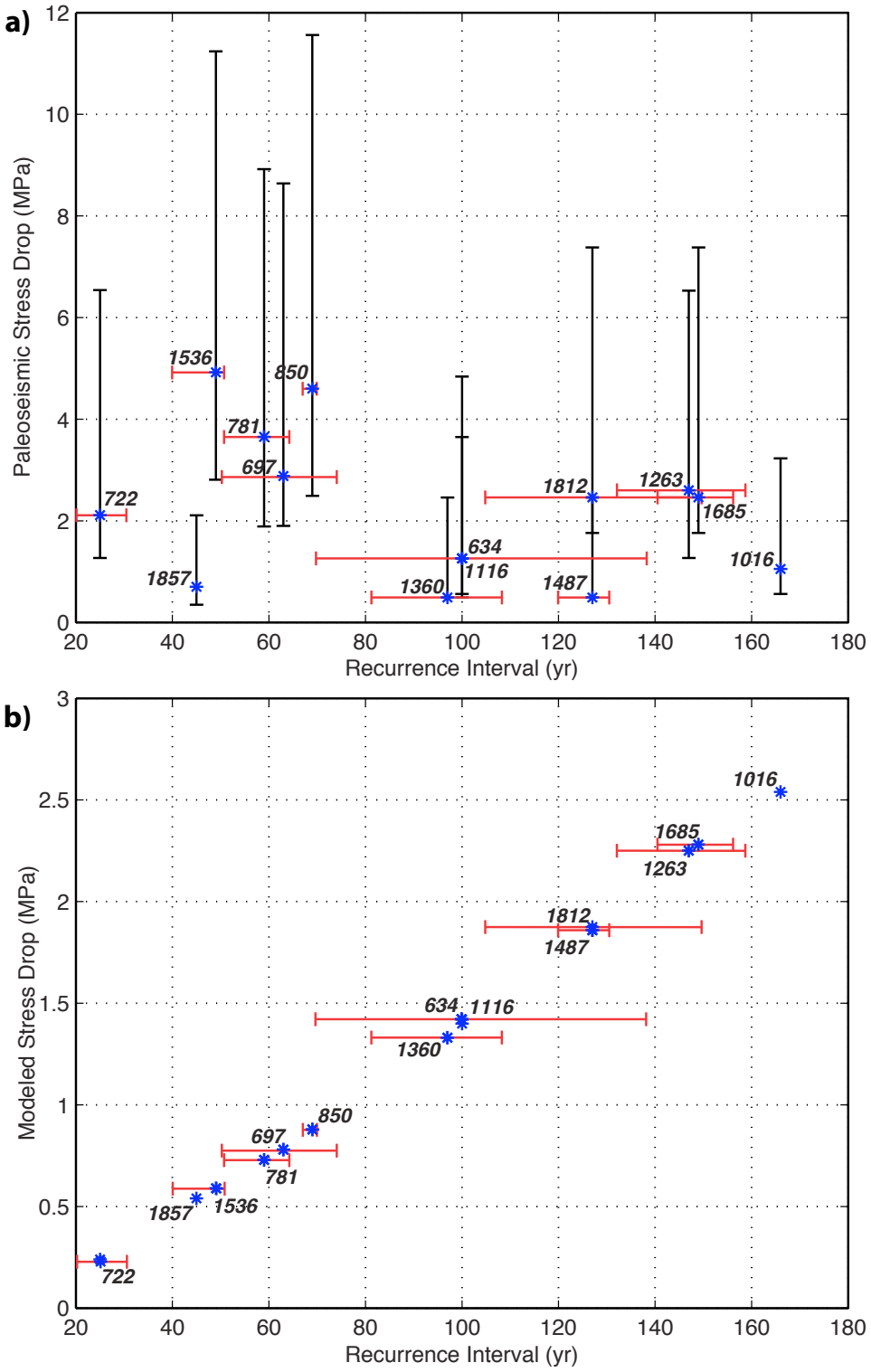

Figure 3.6. a) Paleoseismic stress drop vs. recurrence interval. Vertical error bars represent stress drop from slip uncertainty while horizontal error bars represent uncertainty in recurrence interval (Table 3.1). b) Modeled stress drop vs. recurrence interval. Error bars represent uncertainty in recurrence interval from Table 3.1.

A stress drop inversely proportional to a recurrence interval (as suggested by the data) seems less intuitive, suggesting that stress accumulation rates would need to be highly variable between earthquake cycles. For example, stress accumulation rates would be highest for the events occurring in years 697, 722, 782, 850, and 1536 (recurrence intervals of 63, 25, 59, 69, and 49, respectively) and lowest for events occurring in 1016, 1263, and 1812 (recurrence intervals of 166, 147, and 127, respectively). This concept leads us to further explore variations within the stress drop and stress accumulation rate parameter space, such as the fault locking depth or fault slip rate.

Our first attempt to match the modeled stress drops to the paleoseismic stress drops was to consider a variable slip rate (Appendix 2.A). The simple ratio of displacement over recurrence interval (Table 3.1) provides a range of slip rates for the 14 earthquake cycles. Slip rates estimated from this approach are as low as 6 mm/yr (1487 event) and as high as 143 mm/yr (1536 event), with a mean rate of 48 mm/yr (Table 2.A.1). These extreme ranges in slip rate per earthquake cycle are considered unrealistic, with little geologic evidence supporting such behavior. Thus, we discard the hypothesis that slip rate variations per earthquake cycle are a primary driver in the highly variable stress accumulation process along the Mojave segment. Instead, we next consider the role of variable locking depth per earthquake cycle as a significant factor driving the changing patterns in stress drop and accumulation rate.

3.6 ESTIMATING DEPTH-DEPENDENT STRESS DROP: DATA AND 4-D MODELS

To test a range of viable fault depths, paleosiseimic slip-derived stress drop is calculated for each of the 14 earthquake cycles at 5, 10, 15, 20 and 25 km locking depths. Using this approach, deeper locking depths should yield lower stress accumulation rates than shallow locking depths, given that stress drop is inversely proportional to the square-root of the fault depth (Equation 3.1). Figure 3.7 demonstrates the sensitivity of paleoseismic data-derived stress drop to changing locking depth. For

example, the 1536 event could have had stress drops of 8.35, 4.82, or 3.73 MPa given fault locking depths of 5, 15, or 25, respectively.

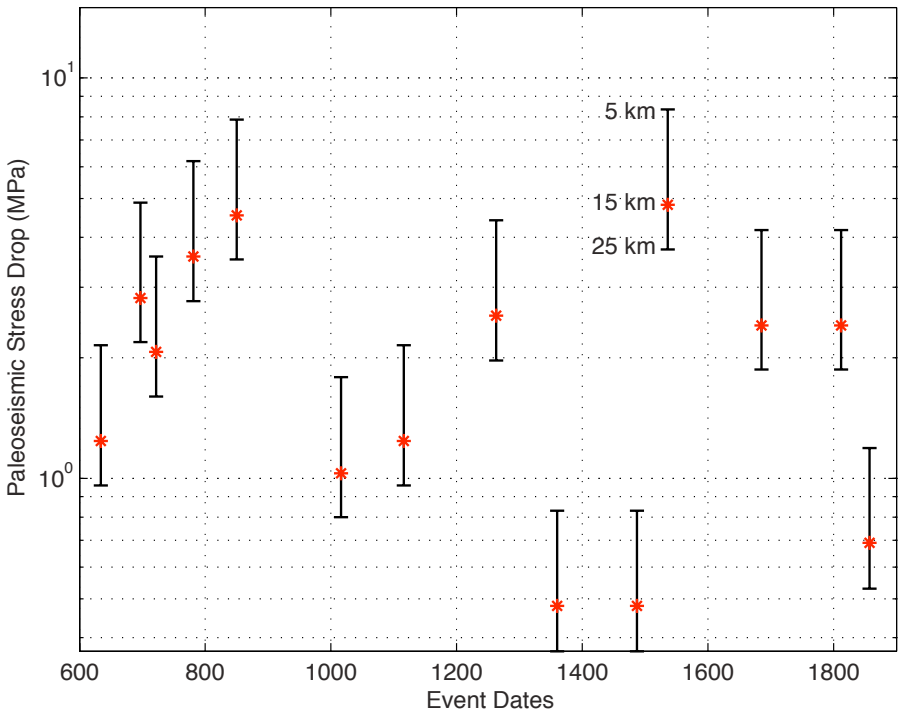

Figure 3.7. Estimated paleoseismic stress drop as a function of fault locking depth. The stars represent the stress drop from the default locking depth of 15 km and error bars represent the upper (5 km depth) and lower (25 km depth) stress rate bounds.

Model-derived stress drop as a function of depth are also estimated using 5-25 km locking depths. As an example, Figure 3.8a shows stress accumulation (and stress drop) snapshots for both the 1812 and 1857 events as a function of fault locking depth. The distribution of stress drop for the 1857 and 1812 events further expresses the dependency of the magnitude of model-derived stress drop with the locking depth and recurrence time. For both events, stress drop decreases with increasing locking depth. Furthermore, the accumulated stress predicted for the 1812 event is consistently higher than that of the 1857 event due to the larger time (127 yrs) between earthquake cycles for the 1812 and 1857 events. From Figure 3.8b, a non-linear relationship between locking depth and stress drop is indicated, where locking depths > 25 km yield a converging low stress rate.

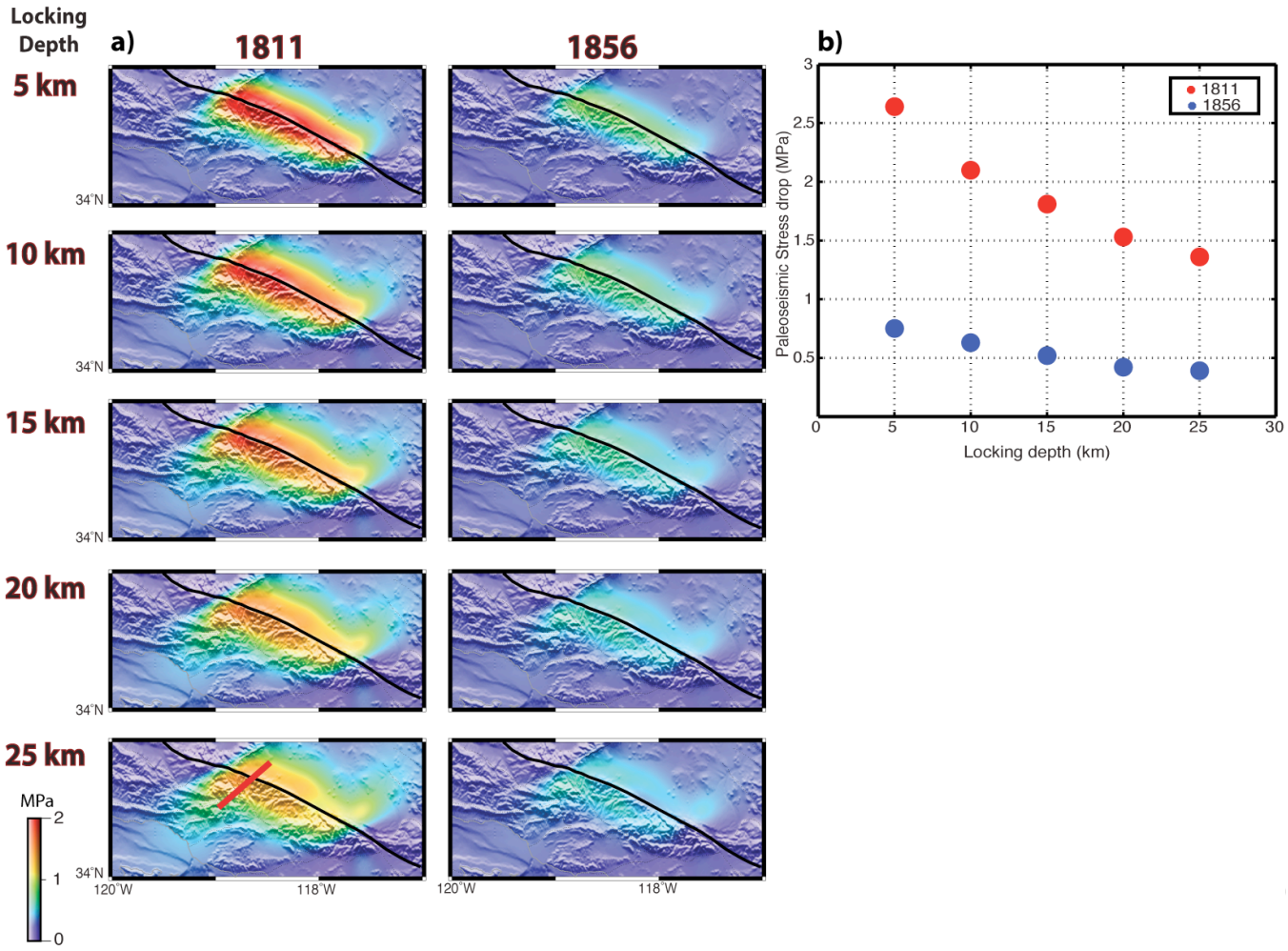

Figure 3.8. Modeled stress accumulation (and inferred stress drop) for the 1812 and 1857 events as a function of locking depth. (a) Map view snapshots of stress accumulation viewed 1 year before each event (approximating coseismic stress drop) for the Mojave segment as a function of fault locking depth. Red line shows the location where stress profile is taken. (b) Model-derived stress drops acquired along a fault-perpendicular transect (a) as a function of fault locking depth.

Modeled stress drops for all 14 earthquake cycles as a function of locking depth are provided in Figure 3.9, which are compared with paleoseismic slip-derived stress drops (from Figure 3.7). We overlay the modeled stress rates from each of the locking depths on top of the paleosesimic stress rates to establish a first order relationship between the two. First, we note that there is a typically larger range of paleoseismic stress drops for each event (for example, 1.87-4.73 MPa for the 1685 event), due to the simple empirically-defined equation adopted for the paleoseismic data; the model predicts a smaller range in stress drop (for example, 1.63-3.09 MPa for the 1685 event), likely due to the more

sophisticated and three-dimensional calculations applied here. Second, we observe two classes of events, one with events that align in magnitude with model-predicted depth range (634, 1116, 1263, 1685, 1812, and 1857), and another class where model stress drops are largely overestimated (697, 722, 781, 850, and 1536) or moderately underestimated (1016, 1360, and 1487). We quantify major outliers by calculating the residual (data – model) mean stress drop (spanning 5-25 km depths) for each event; the 697, 722, 781, 850, and 1536 events yield residual stress drops > 2 MPa, which suggest significant disagreement between data and model-derived stress drops that cannot be explained by significant locking depth variations. We explore alternate scenarios for these events in Section 3.6 and utilize the remaining events (634, 1016, 1116, 1263, 1360, 1487, 1685, 1812, and 1857) to investigate the role of locking depth variations on stress drop.

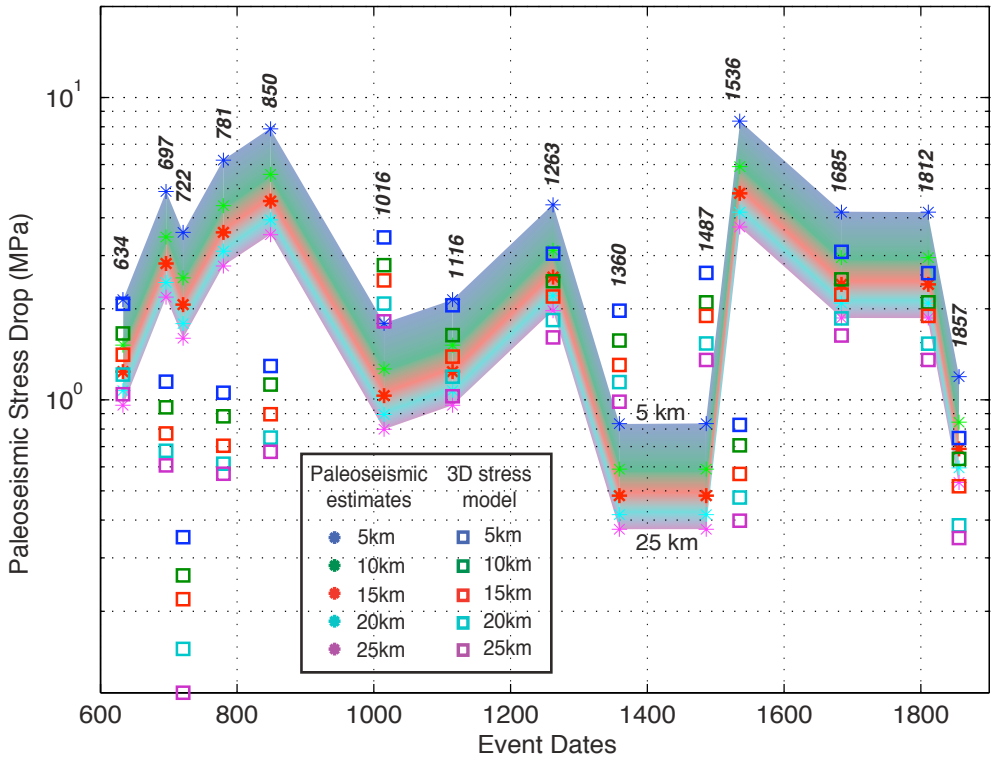

Figure 3.9. Model and paleoseismic slip-derived stress drop as a function of fault locking depth. Colored squares represent model stress drop and colored stars represent paleoseismic data stress drop for 5-25 km locking depth models. The rainbow swath represents the paleoseismic slip-derived stress drop at each of the different locking depths, with colors consistent with those used for the model stress rate symbols.

We next extend these results to determine the best fitting locking depths that minimize the misfit between model- and data-derived stress drop. Individual comparisons of stress drop at 5, 15, and 25 km locking depths are provided in Figure 3.10; however here we also include uncertainties in paleoseismic stress drop from event slip uncertainties (Table 3.1). Several inferences can be drawn from these results. First, these results illustrate the importance of slip uncertainties. For nearly the entire range of tested fault depths (5-25 km), we find that when we accommodate for slip uncertainties, paleoseismic stress drop can be accurately modeled for all 9 events; the single exception to this is the 1812 event using a 5 km locking depth, where the model underestimates the stress drop even for the smallest slip estimate. Second, because the relationship between fault locking depth and stress drop is non-linear, the best fitting depth that minimizes the misfit between model- and data-derived stress drop is not always obvious. Using a 5 km fault locking depth, no minimized misfit between model and data is determined for any of the events, thus this shallow of a locking depth is unlikely to have dominated any of the 9 earthquake cycles. Using a 15 km fault depth, the 1263, 1685, and 1811 events yield minimized stress drop misfit, suggesting that these events stored stress down to a moderate fault depth throughout their earthquake cycles. Lastly, using a 25 km fault depth, stress drop misfits are minimized for the 633, 1016, 1116, 1360, 1487, and 1857 events, suggesting that fairly deep fault locking depths may have played a key role in modulating (lowering) the rate of stress accumulation throughout these earthquake cycles.

Best fitting locking depths for each event are provided in Figure 3.11. Interestingly, minimized stress drop misfits were only determined for 15 km and 25 km depths, although this could be a result of the 5 km depth discretization adopted thus far. From these results, we propose that realistic variations in locking depth spanning 9 of the 14 earthquake cycles of the Mojave segment could have generated enough variation in earthquake cycle stress rate to support non-characteristic stress drop behavior.

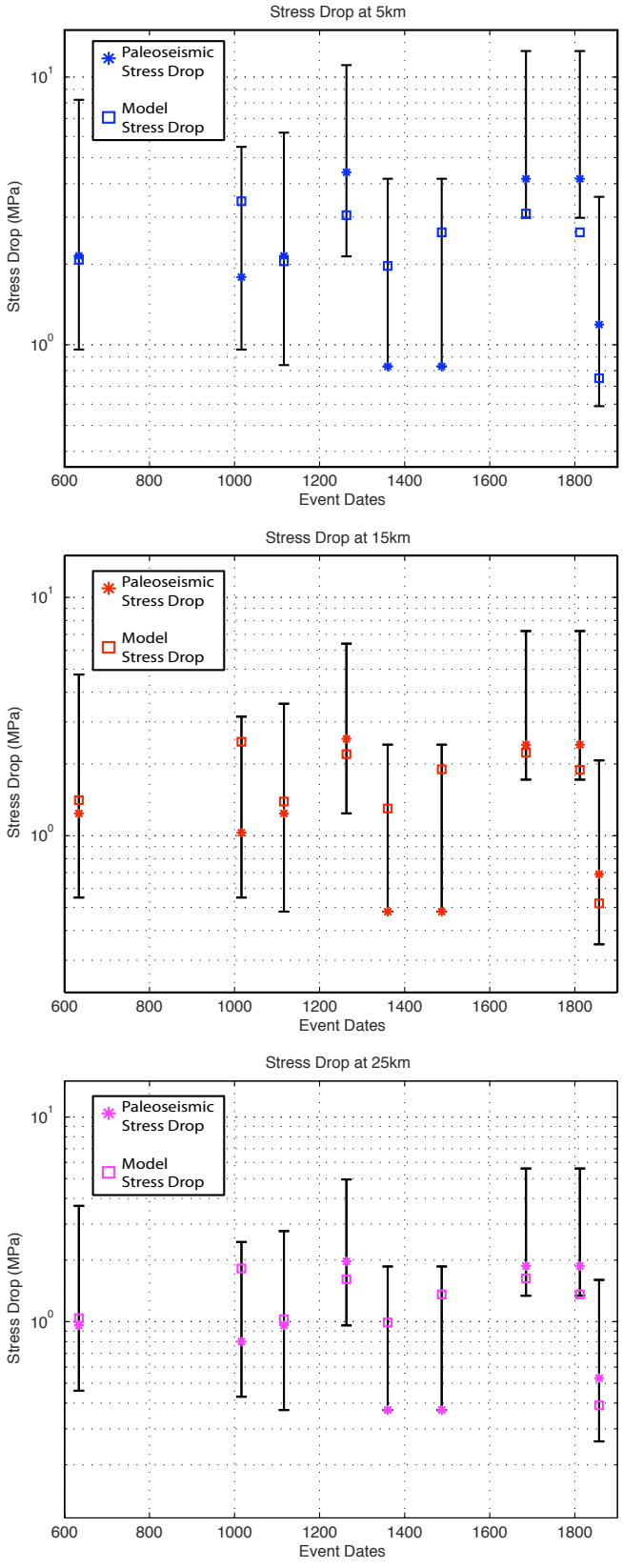

Figure 3.10. Comparison of stress drop from model and paleoseismic data assuming a 5 km, 15 km, and 25 km fault locking depth. Error bars reflect uncertainty in paleoseismic slip (Table 3.1) for each event.

3.7 Discussion: Variation in locking depths, stress rates, and implications for seismic hazards

Stress drops spanning the past 1500 years for the Mojave segment suggest a significant variation in locking depth. Based on the approach and results described in Section 3.5, we determine the best fitting locking depths (5 km increments) (Figure 3.11) by calculating minimized stress drop differences (or residuals) as a function of locking depth for each event. Moderate fault locking depths (~15 km) provide a best fitting paleoseismic data-model match for events that occurred in 1264, 1685, and 1812. Deep fault locking depths (~25 km) fit the data best for the 634, 1016 1116, 1360, 1487, and 1857 events. We cautiously note that higher accuracy calculations (using, perhaps, a 2 km fault depth discretization) will be needed to confirm these results, as a few events yield statistically insignificant variations in misfit using different locking depths.

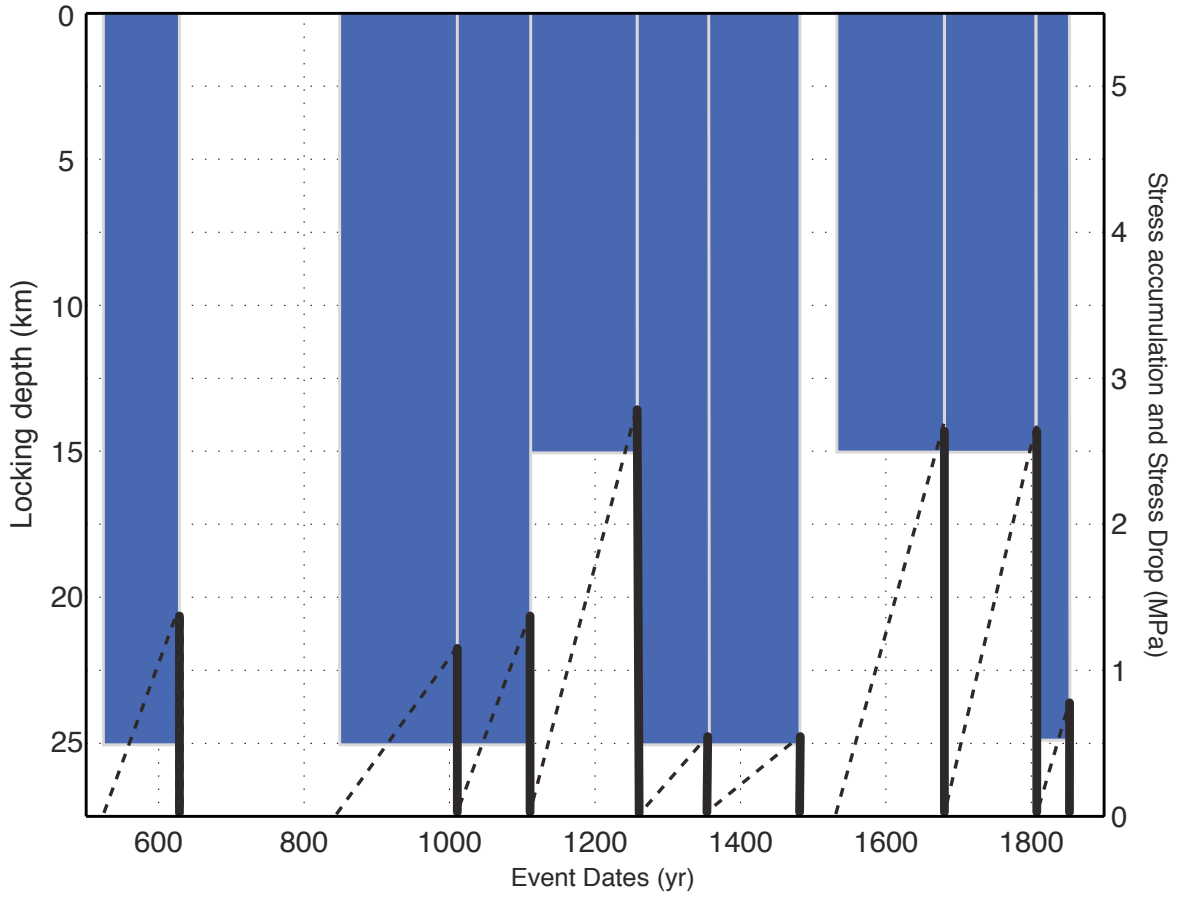

Figure 3.11. Best fitting locking depth per earthquake cycle for the Mojave segment. Stress accumulation and stress drop sequence (using average stress drop determined from a 5-25 km fault depth average) are plotted on the left vertical axis. Outlier events (see Section 3.5) are omitted from this figure.

These results suggest an interesting correlation between event locking depth and stress drop (Figure 3.11). Low stress drop (< ~1.2 MPa) events are best modeled with a larger (25 km) fault depth, while higher stress drop (~ 2.5 MPa) events are best modeled with a moderate (15 km) fault depth. This behavior has also been observed between stress accumulation rate and geodetically-determined locking depths. Low stress accumulation rates are predicted along faults with the deeper locking depths, while high stress rates are predicted along faults with shallow locking depths [*Smith-Konter and Sandwell*, 2009]. In terms of the paleoseismic data, this relationship suggests that when stress is stored by a fault that is more deeply locked, stress will accumulate at a slower rate throughout an earthquake cycle, producing an overall lower stress drop than would be expected for a shallow fault.

While the range of stress drop-inferred locking depths along the Mojave segment may have ranged from 15-25 km over the span of the last 1500 years, we also note an interesting link between the present-day locking depth estimated from modern data and the 1500-year average locking depth computed from this study (19.5 km). This depth is slightly larger than the 16.8 +/- 0.4 km effective geodetic locking depth and the seismically estimated elastic thickness of 13.2 ± 1.2 km for the Mojave segment [*Smith-Konter et al*., 2011]. A shallower than average fault locking depth suggests that the Mojave segment may rupture with a higher than average stress drop and may be presently storing stress at a rate faster that that of the 9-earthquake cycle average.

Using a 15 km locking depth, Figure 3.3 suggests that the accumulated stress today is now approaching ~2.25 MPa. In comparison to past events, today's accumulated stress has surpassed the level estimated for the 1812 event. For a 5 km fault depth, present-day stress accumulation would be increased to 3.25 MPa; for a 25 km fault depth, present-day stress accumulation would be decreased to 1.71 MPa. If we adopt this range of plausible stress drops for an event occurring today, earthquake magnitudes can be estimated using the following relationship between stress drop and moment magnitude,

$$M_o = \frac{w^2 L \pi \Delta\sigma}{2} \quad \textbf{(3.2)}$$

$$M_w = \frac{\log M_o}{1.5} - 6.03 \quad \textbf{(3.3)}$$

where w is the locking depth, L is the length of the segment, and M_o is the seismic moment. For fault depths of 5-25 km, we estimate that the Mojave segment could currently be primed for an 8.0-8.8 magnitude event, assuming a complete segment length rupture.

Finally, we note that five events (occurring between 600-900 A.D. and in year 1536) from the Wrightwood paleoseismic sequence were determined as significant outliers in our locking depth analysis. Paleoseismic stress drops are anomalously high for these events due to shorter than average recurrence intervals (less than 70 years) and larger than average displacements (> 6 m). Realistic variations in locking depth could not be modeled with acceptable stress drop magnitudes, suggesting that an alternative explanation for the occurrence and slip of these events may be needed. We find that the stress rates for these outliers (assuming a 15 km locking depth) is much larger (4.5-9.8 MPa/100 yrs) than for rates inferred from the remaining events (~0.4-1.8 MPa/100 yrs). For these events, *Weldon et al*. [2004] suggest that strain release was ~3 times the average compared to earthquake activity occurring between 800 and 1900 A.D. It is possible that before 600 A.D. anomalously high amounts of strain accumulated over many earthquake cycles (perhaps due to incomplete stress drop mechanisms), resulting in a series of large slip events. A variable slip (or strain) rate for these outlier events is also another option to consider (Appendix 3.A); model-derived stress drops estimated by this approach could double or triple, placing them within range of a data-derived stress drop assuming fairly deep locking depths. To obtain these significantly larger stress drop estimates from our model, however, requires slip rates 2-4 times larger than both geologically and geodetically-determined slip rates, which seems unrealistic.

Fault length is also an uncertain parameter within this analysis. We assume that all events at the Wrightwood paleoseismic site ruptured the same fault length (126.6 km), and while this may be true, there are other plausible scenarios where rupture was limited or extended to smaller or larger sections of the fault [*Fumal et al*., 2002; *Biasi et al*., 2002; *Weldon et al*., 2004]. If rupture occurred over a fault length larger than the 126.6 km assumed here, then paleoseismic-derived stress drop values would decrease according to Equation 3.1 Rupture length does not affect our model-derived stress drop values,

so it is possible that stress drop magnitudes could converge between data and model if we consider variable length ruptures, which will be the focus of a future study.

The obvious clustering of events between 600-900 A.D. may also have modulated the effective elastic properties of the Earth's crust, where the shear modulus may have been reduced throughout these particular earthquake cycles. For example, damage zones surrounding several faults in southern California have been linked to large variations in effective shear modulus [i.e., *Fialko*, 2004; 2006]. For the five outlier events identified in this study, application of a reduced shear modulus would indeed reduce the data-derived stress drop estimates (Equation 3.1), however stress drop and shear modulus also have a linear relationship in the 4-D model, so this would also decrease model estimates as well.

Alternatively, triggered stress from nearby fault segment ruptures may have provided enough stress to encourage unexpected rupture scenarios for the five outlier events. Stress concentrations can vary spatially, particularly near locations of complex fault geometry and interacting fault segments [*Kanamori*, 1994]. The southern end of the Mojave segment lies adjacent to the San Bernardino segment of the San Andreas fault and the San Jacinto Mountains segment of the San Jacinto fault. Triggered rupture scenarios at this junction [*Anderson et al.*, 2003] suggest that a large northern San Jacinto fault rupture event could trigger a Mojave segment rupture similar to the 1812 or 1857 events. Our model does not currently include triggered stress from paleoseismic ruptures along adjacent segments, and thus it is possible that stress contributions from these alternate sources could increase model stress accumulation and stress drop magnitudes along the Mojave segment for particular periods of time.

3.8 CONCLUSIONS

The main objective of this research is to investigate the relationship between stress variations and the temporal occurrence of major earthquakes along the Mojave segment of the SAFS. We investigated the relevance of variable locking depth through time and how this may have caused

significant changes in earthquake cycle stress accumulation and coseismic stress drop. Using the paleoseismic database published for the Mojave segment [*Weldon et al*., 2004], we estimated stress drop for 14 paleoseismic events spanning the last ~1500 years. Similarly, we estimated stress drop for all 14 events using a 4-D earthquake cycle stress model [*Smith-Konter and Sandwell*, 2009], assuming a constant slip rate but variable locking depth for the Mojave segment. We fit the model-derived stress drops for each earthquake cycle to the stress drop estimates derived from paleoseismic offset data to determine the best-fitting locking depth for each of the 14 events.

Assuming a nominal fault depth of 15 km, paleoseismic slip-derived stress drops along the Mojave segment range from 0.49 to 4.92 MPa, with a mean stress drop of 2.21 MPa. Model-derived stress drops range from 0.24 to 2.54 MPa, with a mean stress drop of 1.34 MPa. These first order variations suggest that while we have adopted realistic model parameters for simulating multiple earthquake cycles along the Mojave segment, some refinement of parameter values like slip rate, shear modulus, and fault length, in addition to inclusion of multiple earthquake cycles along adjacent fault segments, may also be warranted. The focus of this study, however, is to understand the role of variable locking depth per earthquake cycle as a significant factor driving the changing patterns in stress drop and accumulation rate.

From our locking depth analysis, we infer two classes of events amongst the Mojave paleoseismic earthquake sequence, one with events that align in magnitude with model-predicted depth range (in years 634, 1116, 1016, 1263, 1685, 1812, and 1857), and another class where model stress drops are largely overestimated (697, 722, 781, 850, and 1536) or moderately underestimated (1016, 1360, and 1487). We quantify major outliers by calculating the residual mean stress drop (spanning 5-25 km depths) for each event; 697, 722, 781, 850, and 1536 yield residual stress drops > 2 MPa, which suggest significant disagreement between data and model-derived stress drops that cannot be explained by significant locking depth variations. For the remaining events, we find that for nearly the entire

range of tested fault depths (5-25 km), when we accommodate for slip uncertainties, paleoseismic stress drop can be accurately modeled. Of these 9 events, fault depths of 15 km best fit stress drops from the 1263, 1685, and 1812 events, while fault depths of 25 km best fit stress drops from the 634, 1016, 1116, 1359, 1486, and 1857 events.

These results suggest an interesting correlation between event locking depth and stress drop, where low stress drop events are best modeled with a larger fault locking depth and higher stress drop events are best modeled with a moderate fault locking depth. In terms of the paleoseismic data, this relationship suggests that when stress is stored by a fault that is more deeply locked, stress will accumulate at slower rate throughout an earthquake cycle, producing an overall lower stress drop than would be expected for a shallow fault. From these results, we propose that realistic variations in locking depth spanning 9 of the 14 earthquake cycles of the Mojave segment could have generated enough variation in earthquake cycle stress rate to support non-characteristic stress drop behavior. Future work will be aimed at exploring the role of incomplete stress drop for the Mojave segment to best simulate anomalous locking depths for several events.

3.9 REFERENCES

Anderson, G., Aagaard, B., and Hudnut, K. (2003), Fault interactions and large complex earthquakes I the Los Angeles area. *Science*, *302*(5652), 1946-1949.

Atwater, T., and Molnar, P. (1973), Relative motion of the Pacific and North American plates deduced from sea-floor spreading in the Atlantic, Indian, and South Pacific Oceans. *Stanford Univ. Publ. Geol. Sci*, *13*, 136-148.

Biasi, G. P., Weldon, R. J., Fumal, T. E., and Seitz, G. G. (2002), Paleoseismic event dating and the conditional probability of large earthquakes on the southern San Andreas fault, California. *Bulletin of the Seismological Society of America*, *92*(7), 2761-2781.

Biasi, G. P., Weldon, R. J., Fumal, T. E., and Seitz, G. G. (2002), Paleoseismic event dating and the conditional probability of large earthquakes on the southern San Andreas fault, California. *Bulletin of the Seismological Society of America*, *92*(7), 2761-2781.

Biasi, G. P., and Weldon, R. J. (2009), San Andreas fault rupture scenarios from multiple paleoseismic records: Stringing pearls. *Bulletin of the Seismological Society of America*, *99*(2A), 471-498.

Fumal, T. E., Pezzopane, S. K., Weldon, R. J., and Schwartz, D. P. (1993), A 100-year average recurrence interval for the San Andreas fault at Wrightwood, California. *SCIENCE-NEW YORK THEN WASHINGTON-*, *259*, 199-199.

Fumal, T. E., Weldon, R. J., Biasi, G. P., Dawson, T. E., Seitz, G. G., Frost, W. T., and Schwartz, D. P. (2002), Evidence for large earthquakes on the San Andreas fault at the Wrightwood, California, paleoseismic site: AD 500 to present. *Bulletin of the Seismological Society of America*, *92*(7), 2726-2760.

Fialko, Y. (2004), Probing the mechanical properties of seismically active crust with space geodesy: Study of the coseismic deformation due to the 1992 Mw7. 3 Landers (southern California) earthquake. *Journal of Geophysical Research: Solid Earth (1978–2012)*, *109*(B3).

Fialko, Y. (2006), Interseismic strain accumulation and the earthquake potential on the southern San Andreas fault system. *Nature*, *441*(7096), 968-971.

Harris, R. A., and Simpson, R. W. (1996), In the shadow of 1857-the effect of the Great Ft. Tejon Earthquake on subsequent earthquakes in southern California.*Geophysical Research Letters*, *23*(3), 229-232.

Harris, R. A. (1998), Introduction to special section: Stress triggers, stress shadows, and implications for seismic hazard. *Journal of Geophysical Research: Solid Earth (1978–2012)*, *103*(B10), 24347-24358.

Harris, R. A., and Simpson, R. W. (1998), Suppression of large earthquakes by stress shadows: A comparison of Coulomb and rate-and-state failure. *Journal of Geophysical Research: Solid Earth (1978–2012)*, *103*(B10), 24439-24451.

Kanamori, H. (1977), The energy release in great earthquakes. *Journal of Geophysical Research*, *82*(20), 2981-2987.

Kanamori, H., and Allen, C. R. (1986), Earthquake repeat time and average stress drop. *Earthquake Source Mechanics*, *37*, 227-236.

Kanamori, H. (1994), Mechanics of earthquakes. *Annual Review of Earth and Planetary Sciences*, *22*, 207-237.

Meade, B. J., and Hager, B. H. (2005), Block models of crustal motion in southern California constrained by GPS measurements. *Journal of Geophysical Research: Solid Earth (1978–2012)*, *110*(B3).

Nazareth, J. J., and Hauksson, E. (2004), The seismogenic thickness of the southern California crust. *Bulletin of the Seismological Society of America*,*94*(3), 940-960.

Ruff, L. J. (1999), Dynamic stress drop of recent earthquakes: Variations within subduction zones. In *Seismogenic and Tsunamigenic Processes in Shallow Subduction Zones* (pp. 409-431). Birkhäuser Basel

Scharer, K. M., Weldon, R. J., Fumal, T. E., and Biasi, G. P. (2007), Paleoearthquakes on the southern San Andreas fault, Wrightwood, California, 3000 to 1500 BC: A new method for evaluating paleoseismic evidence and earthquake horizons. *Bulletin of the Seismological Society of America*, *97*(4), 1054-1093.

Scharer, K. M., Biasi, G. P., Weldon, R. J., and Fumal, T. E. (2010), Quasi-periodic recurrence of large earthquakes on the southern San Andreas fault.*Geology*, *38*(6), 555-558..

Scholz, C. H., and Cowie, P. A. (1990), Determination of total strain from faulting using slip measurements. *Nature*, *346*(6287), 837-839.

Sieh, K., Stuiver, M., and Brillinger, D. (1989), A more precise chronology of earthquakes produced by the San Andreas fault in southern California. *Journal of Geophysical Research: Solid Earth (1978–2012)*, *94*(B1), 603-623.

Smith, B., and Sandwell, D. (2003), Coulomb stress accumulation along the San Andreas Fault system. *Journal of geophysical research*, *108*(B6), 2296.

Smith, B. R., & Sandwell, D. T. (2006), A model of the earthquake cycle along the San Andreas Fault System for the past 1000 years. *Journal of Geophysical Research: Solid Earth (1978–2012)*, *111*(B1).

Smith-Konter, B., and Sandwell, D. (2009), Stress evolution of the San Andreas fault system: Recurrence interval versus locking depth. *Geophysical Research Letters*, *36* (13).

Smith-Konter, B. R., Sandwell, D. T., and Shearer, P. (2011), Locking depths estimated from geodesy and seismology along the San Andreas Fault System: Implications for seismic moment release. *Journal of Geophysical Research: Solid Earth (1978–2012)*, *116*(B6).

Weldon, R. J., Fumal, T. E., Powers, T. J., Pezzopane, S. K., Scharer, K. M., and Hamilton, J. C. (2002), Structure and earthquake offsets on the San Andreas fault at the Wrightwood, California, paleoseismic site. *Bulletin of the Seismological Society of America*, *92*(7), 2704-2725

Weldon, R., Scharer, K., Fumal, T., and Biasi, G. (2004), Wrightwood and the earthquake cycle: What a long recurrence record tells us about how faults work. GSA today, 14(9), 4-10.

Wills, C. J., II, R. W., and Bryant, W. A. (2007), California Fault Parameters for the National Seismic Hazard Maps and Working Group on California Earthquake Probabilities. *US Geological Survey Open File Report*.

Appendix 1 A: Complete Paleoseismic database SAFS PDV2

The following text provides detailed information on our San Andreas Fault System Paleoseismic Database Version 2 (SAFS PDV2). To study the ~400 km long southern half of the San Andreas fault (SAF), we have divided the SAFS into 9 segments (Figure 1.A.1), where each red dot in this figure is located roughly on the center of each of the segments. Exact geographic locations for each study are documented in our SAFS PDV2 as reported in the literature.

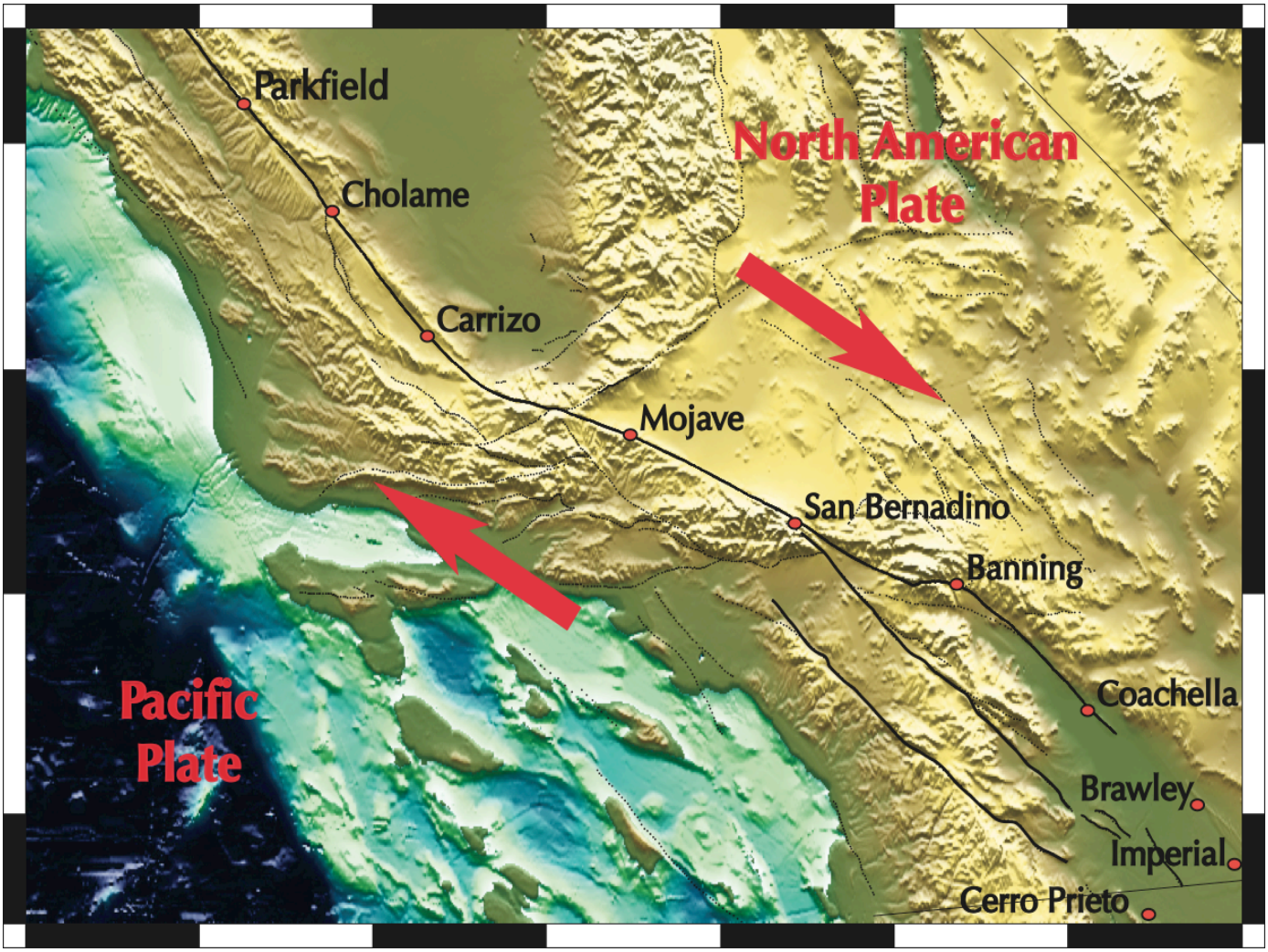

Figure 1.A.1: Regional map of California showing the names of the segments that are included in the SAFS PDV2. Each red dot is located roughly in the center of each segment.

Table 1.A.1. Complete paleoseismic database from Chapter 2. San Andreas Fault System segment names, event dates, authors, title of publications, slip rates and relevant notes from each publication.

San Andreas Fault Segment Names	Event Dates	Authors	Title	Slip Rates (mm/yr)	Notes
Parkfield	1857, 2004	Toke et al., 2009.	Long-lived creep, M6 earthquakes, and a holocene slip rate for the main trace of the San Andreas Fault at Parkfield, CA.	24.5±12/-7	The authors mention another sliprate to the north of the segment of 33
	n/a	Petersen et al., 1994	Fault slip rates and earthquake histories for active Fault in Southern California.	33	36.4/121.0 bitterwater valley
	1881, 1901, 1922, 1934, 1966, 2004	Smith et al., 2006	A model of the earhquake cycle along the San Andreas Fault for the last 1000 yers	40	
	1857, 2004	Biasi et al.,2008	Appendix E: overview of the southern San Andreas Fault model	34±3	
	n/a	Grant et al., 2004	Assimilation of paleoseismic data for earthquake simulation	34±5	
	1881, 1901, 1922, 1934, 1966, 2004	Toke et al., 2006	Reassesment of a slip budget along the Parkfield segment of the San Andreas fault	3 ->25	Slip rate from higway 46 to 48 km to the northwest at slack canyon
	1857, 1881, 1901, 1922, 1934, 1966, 2004	Toke et al., 2006	Paleoseismic and postseismic observations of surfaces slip along the Parkfield segment of the San Andreas Fault	10	Study site @ millers field ** see figure 2 in paper.
Cholame	1857	Dawson et al., 2008	Appendix B: recurrence interval and event age data for type A Fault	4.5±2	Slip rate in most recent event
	n/a	Petersen et al., 1994	Fault slip rates and earthquake histories for active Fault in Southern California.	33.9	
	3700yr	Sieh and Jahns, 1984.	Holocene Activity of the San Andreas Fault at Wallace Creek, California.	34±3	Wallace creek
	13250 yrs	Sieh and Jahns, 1984.	Holocene Activity of the San Andreas Fault at Wallace Creek, California.	35.8+5.4/-4.1	Wallace creek
	n/a	Grant et al., 2004	Assimilation of paleoseismic data for earthquake simulation	34±5	
Carrizo	1280-1340 (1310), 1360-1425(1393), 1540-1630(1585), 1640-1857 (1749), 1857	Akciz et al., 2009	Revised dates of large earthquakes along the Carrizo section of the San Sandreas fault, California, since A.D. 1310 +- 30	n/a	Bidart Fan
	599, 1078, 1277, 1384, 1571, 1857	Biasi et al., 2009	San Andreas Fault rupture scenarios from multiple paleseismic records: "stringing pearls"	n/a	
	1218 - 1276, 1277 - 1510, 1405 - 1510, 1857	Grant et al., 1994	Paleoseismic evidence of clustered earthquakes on the San Andreas fault in the Carrizo Plain, California.	34±3	
	599, 1078, 1277, 1384, 1571, 1857	Dawson et al., 2008	Appendix B: recurrence interval and event age data for type A Fault	7±4	Wallace Creek/Bidart Fan
	n/a	Weldon et al., 2008	Appendix E: overview of the southern San Andreas Fault model	36±2	
	n/a	Grant et al., 2004	Assimilation of paleoseismic data for earthquake simulation	34±3	

	534, 634, 697, 722, 781, 850, 1016, 1116, 1263, 1360, 1487, 1536, 1685, 1812, 1857	Weldon et al., 2004	Wrightwood and earthquake cycle: What a long recurrence record tells us about how faults work		
	534, 634, 697, 722, 781, 850, 1016, 1116, 1263, 1360, 1487, 1536, 1685, 1812, 1857	Sharer et al., 2007	Paleoearthquakes on the Southern San Andreas Fault, Wrightwood, California, 3000 to 1500 B.C.: A new model fro evaluating paleoseismic evidence and earthquake horizons.		
	1857, 1812, 1465-1695, 1329-1363, 1035-1165, 1015-1081, 981-1013, 775-919, 721-747, 658-684	Petersen et al., 1994	Fault slip rates and earthquake histories for active Fault in Southern California.	35.2-35.8	Pallet Creek
	614-666, 749-775, 803-868, 914-986, 1031-1096, 1046-1113, 1343-1370, 1496-1599, 1812, 1857	Grant et al., 2002	Introduction to the special issue on paleoseismology of the San Andreas fault system.		Pallet Creek
	1503… BC dates here	Scharer et al., 2007	Paleoearhquakes on the Southern San Andreas Fault, Wrightwood, California 3000 to 1500 BC: A new method for evaluating paleoseismic evidence and earthquake horizons	40	
	533, 634, 697, 722, 781, 850, 1016, 1116, 1264, 1360, 1487, 1536, 1685, 1812, 1857	Biasi et al., 2009	San Andreas Fault rupture scenarios from multiple paleoseismic records: "stringing pearls"	n/a	Wrightwood
	1812, 1857	Weldon et al., 2008	Appendix E: overview of the southern San Andreas Fault model	32 - 38	North segment
	1812, 1857	Weldon et al., 2008	Appendix E: overview of the southern San Andreas Fault model	28.7	South segment
Mojave	407-628, 551-681, 657-722, 695-740, 736-811, 800-881, 957-1056, 1047-1181, 1191-1305, 1448-1518, 1508-1569, 1647-1717, 1812, 1857	Fumal et al, Biasi et al and Weldon et al in Grant et al., 2002	Introduction to the special issue on paleoseismology of the San Andreas fault system.	20-40	Wrightwood
	533, 634, 697, 722, 781, 850, 1016, 1116, 1264, 1360, 1487, 1536, 1685, 1812, 1857	Dawson et al., 2008	Appendix B: recurrence interval and event age data for type A Fault	6±2	Wrightwood
	n/a	Petersen et al., 1994	Fault slip rates and earthquake histories for active Fault in Southern California.	48	Three Points
	645, 764, 842, 956, 1067, 1084, 1360, 1547, 1812, 1857	Biasi et al., 2009	San Andreas Fault rupture scenarios from multiple paleoseismic records: "stringing pearls"	n/a	
	690, 740, 800, 1000,1050, 1300, 1370, 1500, 1812, 1857	Yeats et al., 1990	Paleoseismicity: extending the record of earthquakes into prehistoric time	n/a	Dates are averages of the ranges shown on figure 1.
	1856	Bennet et al., 1996	Global positioning system constraints on fault slip rates in southern California and northern Baja, Mexico	35±2	Locking depth 12km
	1857	Johnson et al., 2007	Influence of lithosphere viscosity structure on estimates of fault slip rate in the Mojave region of the San Andreas Fault	25-35	14 events in the last 1600 years. Probability distributions for timing of past earthquakes at the three sites labeled in figure 1.
	533, 634, 697, 722, 781, 850, 1016, 1116, 1264, 1360, 1487, 1536, 1685, 1812, 1857	Smith et al., 2006	FaultA model of the earthquake cycle along the San Andreas Fault Systemfor the last 1000 years	40	
	n/a	Weldon et al., 2009	Slip rate on the San Andreas Fault near little rock, CA.	20-40	

	Early Eocene	Behr et al., 2009	Uncertainties in slip rate estimates for the Mission Creek strand of the southern San Andreas Fault at Biskra Palms Oasis.	12, 22	Dating technique explain, 2008 SCEC abstracts
		Bennet et al., 1996	Global positioning system constraints on fault slip rates in southern California and northern Baja, Mexico	26±1	Locking depth 12 km
	n/a	Grant et al., 2004	Assimilation of paleoseismic data for earthquake simulation	25±5	
	1350, 1690	Smith et al., 2006	A model of the earthquake cycle along the San Andreas Fault for the last1000 years	28	
		Rust, 2005	Paleoseismology in steep terrain: the Big Bend of the San Andreas Fault, Transverse Ranges, CA	n/a	
	824, 982, 1230, 1503, 1683	Dawson et al., 2008	Appendix B: recurrence interval and event age data for type A Fault	n/a	Thousand Palms oasis
	770-890, 840-1150, 1170-1290, 1450-1555, 1520-1680	Fumal et al in Grant et al., 2002	Introduction to the special issue on paleoseismology of the San Andreas fault system.	4±2	Thousand Palms Oasis
	824, 982, 1230, 1503, 1683	Biasi et al., 2009	San Andreas Fault rupture scenarios from multiple paleoseismic records: "stringing pearls"	n/a	thousand palms oasis
	n/a	Fumal et, at in Van der Woerd, 2008	Long-term slip rate of the southern San Andreas Fault from 10Be-26Al surface exposure dating of an offset alluvial fan	4±2	Thousand Palms oasis
Coachella	n/a	Van der Woerd, 2008	Long-term slip rate of the southern San Andreas Fault from 10Be-26Al surface exposure dating of an offset alluvial fan Appendix B: recurrence interval and event age data for type A Fault	15.9±3.4	Indio
	n/a	Keller et. Al, in Van der Woerd, 2008		10, 35	Indio
	1020, 1300, 1480, 1680	Dawson et al., 2008		n/a	Indio
	1020, 1300, 1480, 1680	Biasi et al., 2009	San Andreas Fault rupture scenarios from multiple paleoseismic records: "stringing pearls"	n/a	Indio
	1680	Hudnut et al. 2009	Recent offset measurements, Coachella Valley Segment, San Andreas Fault	16±1	
	3400 yr	Shifflett et al 2002 in Van der Woerd et al 2006	Long-term slip rate of the southern San Andreas Fault from 10Be-26Al surface exposure dating of an offset alluvial fan	6.5±1.5	Mecca Hills
	900 yr	Williams 1989 and Sieh and Williams et al 1990 in Van der Woerd 2006	Long-term slip rate of the southern San Andreas Fault from 10Be-26Al surface exposure dating of an offset alluvial fan	9±2	Salt Creek
	1020±A.D., 1300 ±90 A.D., 1450 ±150 A.D.,1680 ±40 A.D.	Petersen et al., 1994	Fault slip rates and earthquake histories for active Fault in Southern California.	23-35	Indio

San Bernardino	n/a	Grant et al., 2004	Assimilation of paleoseismic data for earthquake simulation	24±6	
	931, 1173, 1313, 1437, 1704, 1812	Dawson, Weldon, Biasi, 2008.	Appendix B: recurrence interval and event age data for type A Fault	n/a	Pitman canyon
	1499, 1619, 1812	Dawson, Weldon, Biasi, 2008.	Appendix B: recurrence interval and event age data for type A Fault	n/a	Plunge creek
	1450, 1510-1730	Grant et al., 2002	Introduction to the special issue on paleoseismology of the San Andreas fault system.	n/a	Plunge creek
	220 yrs	Weldon et al., 2008	Appendix E: overview of the southern San Andreas Fault model	25	Cajon creek
	1500 yr	Weldon and Sieh 1985 in van der Woerd, 2008.	Long-term slip rate of the southern San Andreas Fault from 10Be-26Al surface exposure dating of an offset alluvial fan	24.5±3.5	Cajon Pass
	n/a	McGill et al., 2008	Preliminary slip rates along the San Bernardino strand of the San Andreas Fault	25	Cajon Pass
	1948, 1986	Weldon et al., 200	Appendix E: overview of the southern San Andreas Fault model.	n/a	
	1360-1690, 1812, 1857	Rust, 2005	Paleoseismology in steep terrain; The Big Bend of the San Andreas fault, Transverse Ranges, California	34	
	last 14k years	Harden et al., 2010	Holocene and late Pleistocene slip rates on the San Andreas fault in Yucaipa California, using displaced alluvial-fan deposits and soil chronology	35	Yucaipa
	774, 1107, 1347, 1475, 1500, 1684, 1812	Biasi et al., 2009	San Andreas Fault rupture scenarios from multiple paleoseismic records: "stringing pearls"	n/a	Burro flats
	774, 1107,1347, 1475, 1500, 1684, 1812	Dawson et al., 2008	Appendix B: recurrence interval and event age data for type A Fault		Burro Flats
	n/a	Bennet et al., 1996	Global positioning system constraints on fault slip rates in southern California and northern Baja, Mexico	22±2	Perpendicular slip rate: 13 +-1 Locking Depth 12 km
	1857, 1812, 1700, 1610, 1470	Petersen et al., 1994	Fault slip rates and earthquake histories for active Fault in Southern California.	24	2 to 4 events between 1290 and 1805 A.D
Brawley	171 0, 1940, 1979	Meltzner et al., 2008	Recent and long-term behavior of the Brawley Fault Zone, Imperial Valley California: An Escalation I slip rate?	2	
	1906	Meltzner et al., 2004	Late Holocene earthquake history of the Imperial and Brawley Fault, Imperial Valley, California.	n/a	
	n/a	Bennet et al., 1996	Global positioning system constraints on fault slip rates in southern California and northern Baja, Mexico	23±1	Perpendicular Slip Rate: -12 +-1 Locking Depth: 7.5 km
	Since ~830 AD, every 115 to 430 years	Brothers et al., 2009	Earthquake and lake history beneath the Salton Sea	1.1 to 3.4	

Table 1.A.2. Paleosesimic database for Imperial and Cerro Prieto faults.

Imperial and Cerro Prieto	Event Dates	Authors	Article	Slip Rates (mm/yr)	Notes
Imperial	1500-1600, 1650, 1700, 1940, 1979	Meltzner et al., 2004	Late Holocene slip on the imperial fault, mesquite basin, Imperial Valley CA	~10	SCEC 2008 abstract volume
	1979	Dawson et al., 2008	Appendix B: recurrence interval and event age data for type A Fault	0.18	
	1525, 1575, 1650, 1700, 1940, 1979	Meltzner et al., 2006	Recent and long term behavior of the Brawley Fault Zone. Imperial Valley California: An escalation in slip rate?	2	
	n/a	Bennet et al., 1996	Global positioning system constraints on fault slip rates in southern California and northern Baja, Mexico	35±2	
	n/a	Thomas and Rockwell in Van der Woerd 2008	Long-term slip rate of the southern San Andreas Fault from 10Be-26Al surface exposure dating of an offset alluvial fan	15-20	
	1700, 1906, 1915, 1940, 1979	Meltzner et al., 2004	Late Holocene earthquake History of the Imperial and Brawley Fault, Imperial Valley, California.	n/a	The 1906 eq was in Brawley
	1670, 1875, 1906, 1940, 1979	Le et al., 2008	Spatial and temporal slip rate variability on the San Jacinto Fault	40	
	n/a	Petersen et al., 1994	Fault slip rates and earthquake histories for active Fault in Southern California.	15-20	Lake Cahuilla
	1875, 1940, 1979	Anderson etal., 1997	Earthquake recurrence models and historical seismicity in the Mexicali-Imperial Valley	n/a	Figure 3. Histogram of a number of events by magnitude from 1906 to 1983
	n/a	Grant et al., 2004	Assimilation of paleoseismic data for earthquake simulation	20±5	
Cerro Prieto	1825, 1915, 1927, 1934, 1980	Anderson et al., 1997	Earthquake recurrence models and historical seismicity in the Mexicali-Imperial Valley	n/a	Northern Cerro Prieto
	n/a	Bennet et al., 1996	Global positioning system constraints on fault slip rates in southern California and northern Baja, Mexico	42±1	Locking Depth: 6 km
	1981, 1934, 1966	Anderson etal., 1997	Earthquake recurrence models and historical seismicity in the Mexicali-Imperial Valley	n/a	Southern Cerro Prieto

Table 1.A.3. Paleosesimic database for San Jacinto fault.

SJF Segment Names	Event Dates	Authors	Article	Slip Rates (mm/yr)	notes
Northern San Jacinto	1923	Doser, 1992	Historic Earthquakes (1918 to 1923) and assessment of source parameters along the San Jacinto Fault System.	n/a	
	161, 683,	Fumal et al., 2008	Photomosaics of Trenches at the Walnut site, San Jacinto Fault, San Bernardino, California.	n/a	USGS SHEET B.C. dates: 1438, 1371, 1167, 1067.
Anza/Clark	n/a	Le et al., 2008	Spatial and temporal slip rate variability on the San Jacinto Fault	4.6±1.6 - 7.7 ±1.8	Clark Fault / SCEC 2008 abstracts volume p.166
	0.5-0.6 Ma	Janecke et al., 2009	High geologic slip rates since Early Pleistocene initiation of the San Jacinto and San Felipe Fault Zones in the San Andreas Fault Systems:: Southern California, USA	>-10.2 +6.9/-3.3	SCEC abstracts volume 2008
	n/a	Petersen et al., 1994	Fault slip rates and earthquake histories for active Fault in Southern California.	17	
	25-160, 160-305, 375-555, 995-110, 1075-1205, 1260-1325, 1285-1380, 1305-1400, 1530-1630, 1775-1805	Dawson et al., 2008	Appendix B: recurrence interval and event age data for type A Fault		Hog Lake
	n/a	Petersen et al., 1994	Fault slip rates and earthquake histories for active Fault in Southern California.	12	Hog Lake
	1000, 1410, 1570, 1800	Rockwell, 2006.	The long record of San Jacinto Fault paleoearhquakes at Hog Lake: implications for regional patterns of strain release in the Southern San Andreas Fault System.	16	Hog Lake
	1020, 1230, 1290, 1360, 1630, 1760	Smith et al., 2006	A model of the earthquake cycle along the San Andreas Fault System for the past 1000 years	12	
Coyote Creek	1968	Petersen et al., 1994	Fault slip rates and earthquake histories for active Fault in Southern California.	35.2-35.8	
	n/a	Le et al., 2008	Spatial and temporal slip rate variability on the San Jacinto Fault	12.4±3.5	SCEC 2008 abstracts volume p.166
	1892, 1968	Smith et al., 2006	A model of the earthquake cycle along the San Andreas Fault System for the past 1000 years	12	
	1942, 1954, 1968, 1969, 1987	Bent et al., 1991	A re-examination of historic earthquakes in the san Jacinto Fault zone, California	n/a	
	0.8-0.9 Ma	Janecke et al., 2009	High geologic slip rates since Early Pleistocene initiation of the San Jacinto and San Felipe Fault Zones in the San Andreas Fault Systems:: Southern California, USA	~4.7±1.6	slip rate calculated from ~3.5 +- 1.3 km since ~.8-.9 Ma
Borrego	1968	Petersen et al., 1994	Fault slip rates and earthquake histories for active Fault in Southern California.	3.2	
	1892, 1968	Smith et al., 2006	A model of the earthquake cycle along the San Andreas Fault System for the past 1000 years	12	

Table 1.A.4. Paleosesimic database for Elsinore fault.

Elsinore Segment Names	Event Dates	Authors	Article	Slip Rates (mm/yr)	Notes
Whittier	n/a	Petersen et al., 1994	Fault slip rates and earthquake histories for active Fault in Southern California.	2.5 - 3.0	
	207	Dawson et al., 2008	Appendix B: recurrence interval and event age data for type A Fault	1.9±.01	
	n/a	Dawson et al., 2008	Appendix F: summary of geologic data and development of a priori rupture models for the Elsinore, San Jacinto and Garlock Fault.	2.5 - 3.0	
Glenn Ivy North	0.5-0.6 Ma	Janecke et al., 2009	High geologic slip rates since Early Pleistocene initiation of the San Jacinto and San Felipe Fault Zones in the San Andreas Fault Systems:: Southern California, USA	4.8-5.9	SCEC abstracts volume 2008
	963, 1230, 1283, 1440, 1627, 1910	Dawson et al., 2008	Appendix B: recurrence interval and event age data for type A Fault	0.25	
	1280, 1850, 1910	Dawson et al., 2008	Appendix F: summary of geologic data and development of a priori rupture models for the Elsinore, San Jacito and Garlock Fault.	5.3-5.9	
Temecula	1655-1810	Dawson et al., 2008	Appendix B: recurrence interval and event age data for type A Fault	n/a	4500, 3500, 3000, 2700 BC
	1655-1810	Dawson et al., 2008	Appendix F: summary of geologic data and development of a priori rupture models for the Elsinore, San Jacito and Garlock Fault.	5±2	
Agua Tibia	1655, 1680, 1753, 1804	Vaughan et al., 1999	Paleoseismology of the Elsinore Fault at Agua Tibia Mountain, Southern california.		
	1360 to 1660 A.D., 1260 to 1275 A.D	Petersen et al., 1994	Fault slip rates and earthquake histories for active Fault in Southern California.	2.9-4.9	1300 A.D and 1060 A.D are preferred
Julian	n/a	Dawson et al., 2008	Appendix F: summary of geologic data and development of a priori rupture models for the Elsinore, San Jacito and Garlock Fault.	2.5 - 3	
Wildomar	n/a	Petersen et al., 1994	Fault slip rates and earthquake histories for active Fault in Southern California.	4.2	
Coyote Mountains	n/a	Dawson et al., 2008	Appendix F: summary of geologic data and development of a priori rupture models for the Elsinore, San Jacito and Garlock Fault.	4±1	
	1650, 1892	Dawson et al., 2008	Appendix B: recurrence interval and event age data for type A Fault	1.5±.5	
	n/a	Bennet et al., 1996	Global postioning system consraints on fault slip rates in southern California and northern Baja, Mexico	6±2	Locking Depth 7.5 km
	n/a	Fletcher et al., 2008	Long-term slip rates of the Elsinore-Laguna Salalda Fault, Southern Californa by U-series dating of pedogenic carbonate in progressivelu offset Alluvial fan remnants	2±.2	SCEC abstracts volume 2008
	n/a	Petersen et al., 1994	Fault slip rates and earthquake histories for active Fault in Southern California.	4	

Appendix 2 A: Stress drop variations on the Mojave segment for the past 1500 years using a variable slip rate

To investigate the stress drop variations on the Mojave segment, we also performed a first order evaluation of model-derived stress drop using variable slip rates throughout the 1500-year sequence of events. We note that the results of our primary study assume a constant geologic slip rate of 33 mm/yr [*Weldon et al,* 2004]. Variable slip rates to be applied to the model were calculated using the slip per event and the recurrence intervals listed in Table 2.A.1 (a modified version of Table 3.1 from *Weldon et al*. [2004]). Slip rates estimated from this approach are as low as 6 mm/yr (1487 event) and as high as 143 mm/yr (1536 event), with a mean rate of 48 mm/yr. These ranges in slip rate per earthquake cycle are considered unrealistic, with little geologic evidence supporting such behavior. However, we pursue variations in this parameter to further inspect the relationship of model-derived stress drops and stress drops derived empirically.

For the modeling exercise, just as in the primary study (Chapter 3), we maintain a constant fault depth of 15 km and also make a simplifying assumption that complete stress release (i.e., all stress that has accumulated) occurs along the Mojave segment at years indicated by the earthquake event dates from Table 2.A.1. For this case however, we apply a different slip rate for each earthquake cycle, consistent with those calculated in Table 2.A.1. Stress accumulation (and subsequent stress drop) is calculated for the entire earthquake history of the Mojave segment (Figure 2.A.1), beginning with a first event in year 634 and cycling forward to year 1857 (the 534 event is excluded from our analysis because of its incomplete time interval). As expected, model-derived estimates of stress accumulation (and drop) are very sensitive to slip rate.

Table 2.A.1. From Weldon et al (2004). Information used to calculate a variable slip rate for the Mojave segment. D_{min} and D_{max} are the lowest and highest slip values listed in the uncertainty bracket. The slip is listed in centimeters and the slip rate is listed in millimeters per year. The five events that were identified as obvious outliers (Section 3.5) are highlighted in bold text.

Event date	Recurrence interval	D_1 (cm)	D_{min} (cm)	D_{max} (cm)	Variable slip rate (mm/yr)
1857	45	100	50	200	22
1812	127	350	100	700	28
1685	149	350	100	700	23
1536	**49**	**700**	**300**	**900**	**143**
1487	127	70	0	280	6
1360	97	70	0	280	7
1263	147	370	190	560	25
1116	100	180	110	340	18
1016	166	150	70	310	9
850	**69**	**660**	**300**	**990**	**96**
781	**59**	**520**	**250**	**750**	**88**
722	**25**	**300**	**120**	**630**	**120**
697	**63**	**410**	**140**	**820**	**65**
634	100	180	100	510	18
534	-	190	100	380	

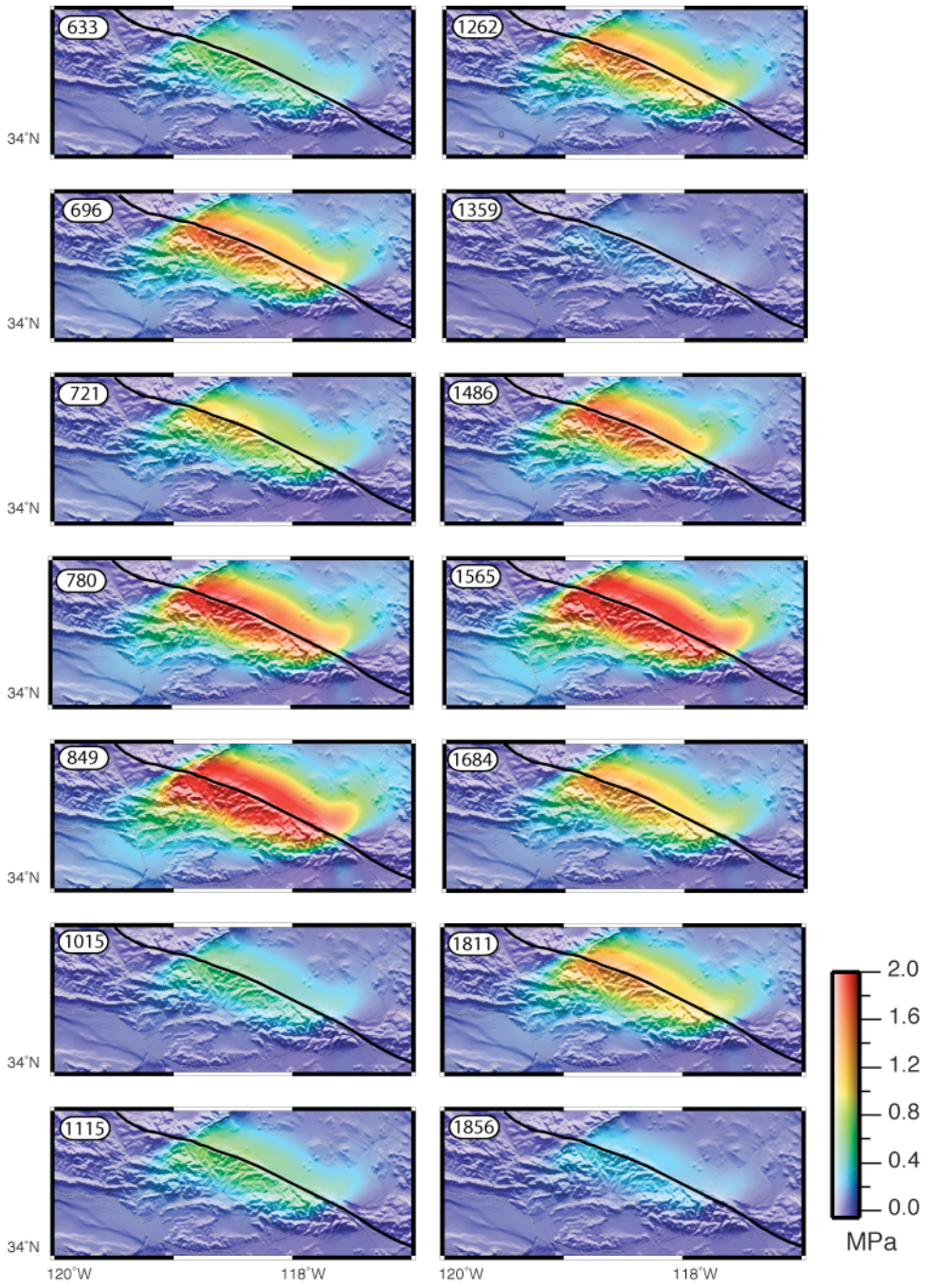

Figure 2.A.1. Snapshots of stress accumulation (approximating coseismic stress drop) for the Mojave segment, estimated using a variable slip rate from Table 2.A.1 and a locking depth of 15 km. Stress accumulation is shown for the year preceding each estimated earthquake event year (Table 2.A.1).

Earthquake stress drop has been empirically estimated by various studies using the ratio of the coseismic fault slip to an appropriate scale length (fault length, fault depth, or the entire fault area)

[*Kanamori*, 1994] over which the slip occurred. It was not initially obvious which scale length was the most appropriate for comparing our model-derived stress drop estimates to, so we evaluated the results from all three. The first scale length we tested utilizes the along-strike length (***L***) of a fault segment to determine the stress drop for each seismic event. We call this the ***L*** relationship and use the following equation:

$$\Delta\sigma = \mu\frac{\overline{D}}{L} \qquad \textbf{(1)}$$

where μ is the crustal shear modulus with an assumed value of 30 GPa; $\overline{D}$ represents event slip (represented by the slip reported in Table 3.1).

The second scale length we tested utilizes the depth (**W**) of a fault segment. We call this the ***W*** relationship and use the following equation:

$$\Delta\sigma = \mu\frac{\overline{D}}{W} \qquad \textbf{(2)}$$

The difference between these two models is that in the *L* relationship, the fault segment is unrestrained both at the top and bottom and in the *W* relationship, the fault segment is locked at the base (Figure 3.4); in the *L* relationship, the stress drop decreases with respect to the length and in the *W* relationship the stress drop is expected to remain constant with respect to the length [*Scholz*, 1982].

The third scale length we tested is called the *LW* relationship and uses the square root of the area (length times width) of the fault:

$$\Delta\sigma = \mu\frac{\overline{D}}{\sqrt{L \cdot W}} \qquad \textbf{(3)}$$

As a result of the rheology around the fault, the stress accumulation is not uniform and this model allows an estimation of the spatial average of the stress drop. This model is the version we adopt throughout the main study.

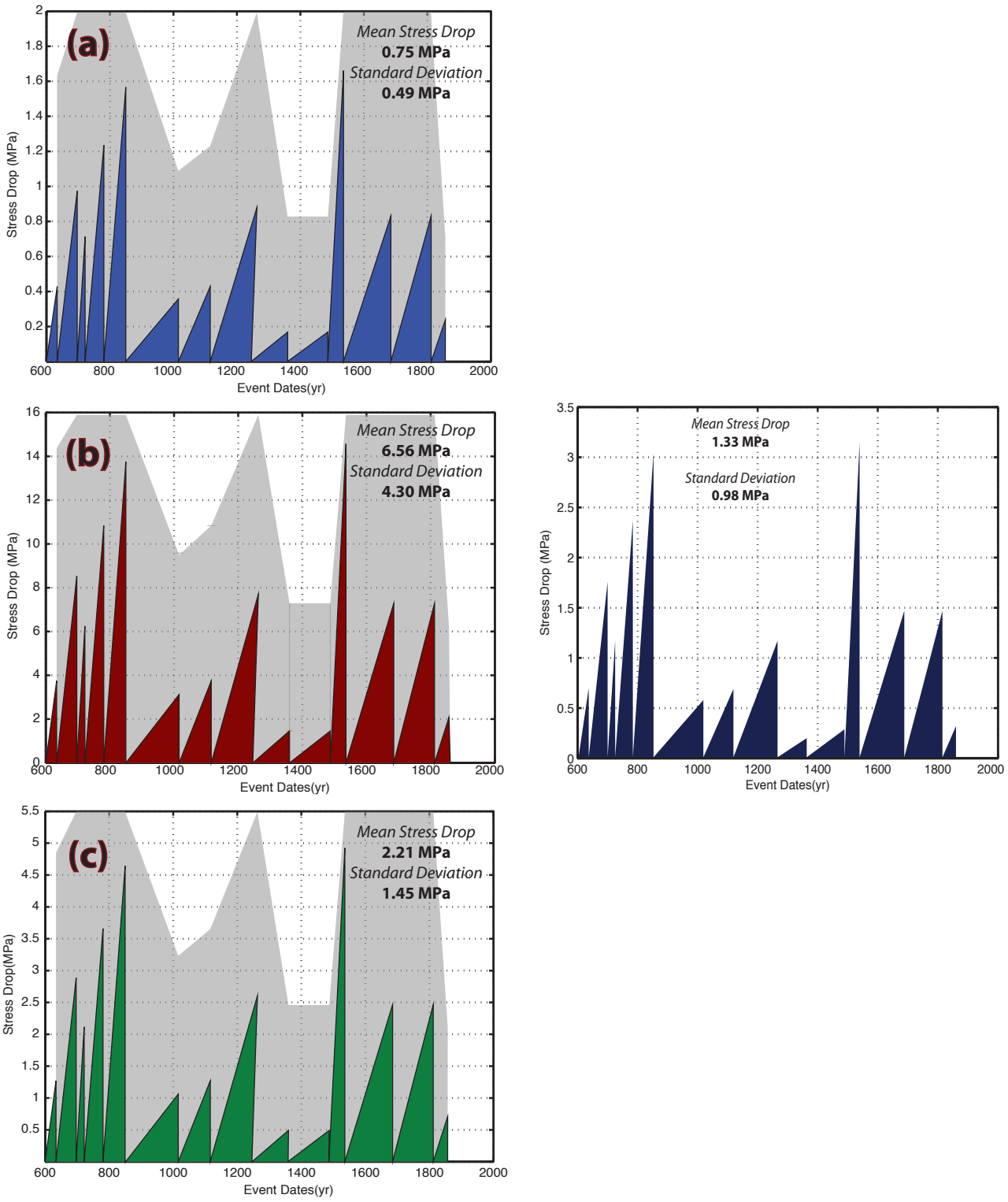

Figure 2.A.2: Left: Paleoseismic slip-derived stress accumulation and drop for the Mojave segment using a fixed slip rate. (a) L relationship. (b) W relationship. (c) LW relationship. Right: Model-derived stress accumulation and drop using variable slip rates from Table 2.A.1.

Figure 2.A.2 (left) illustrates the results of these three empirically derived equations in determining paleoseismic stress drop. The top row shows the stress drop values calculated using the L relationship (mean = 0.75 MPa, std. dev. = 0.49 MPa), the middle row shows values calculated using the W relationship (mean = 6.56 MPa, std. dev. = 4.30 MPa), and the bottom row shows the stress drop using the LW relationship (mean = 2.21 MPa, std. dev. = 1.45 MPa). The stress drop differences between the L and the W relationships are roughly an order of magnitude different. This is because the length of the fault is over 100 km long and the depth is ~ 10 km deep.

Figure 2.A.2 (right) illustrates the model-derived stress drop magnitudes, assuming a variable slip rate for each earthquake cycle. Note that the temporal pattern of stress drop is identical for these models (as opposed to an assumed constant slip rate model, as in Figure 3.5) because we adopted slip rates that could exactly tune the model to replicate this pattern. The stress drop magnitudes shown in this figure range from 0.31-3.14 MPa (mean = 1.33 MPa, std. dev = 0.98 MPa).

To evaluate which empirical relationship provides the best order-of-magnitude stress drop results to those determined by our model, we constructed scatter plots of these quantities (Figure 3.A.3). Results assuming a constant slip rate are also provided for comparison. When a constant slip rate is assumed, there is no obvious correlation between paleoseismic and model-derived stress drops; however, when the model's slip rate is tuned to match slip amounts consistent with paleoseismic estimates, a linear relationship is revealed, where the L, W, and LW scale lengths define the slope of this relationship (a 1:1 ratio of data- to model-derived stress drops would represent the ideal case). For the W relationship, model-derived stress drops are overestimated by those from the data by a 1:5 ratio, or with a slope of 0.2. For the L relationship, model-derived stress drops are underestimated by those from the data with a slope of 1.9. For the LW relationship, model-derived stress drops are slightly overestimated by those from the data with a slope of 0.6.

From these results, we opted to utilize the LW relationship for comparing model and data-derived stress drops. First, the LW relationship provides a closest match to an ideal 1:1 ratio (slope of 1). Second, the LW relationship, as opposed to the L relationship, allows us to explore variations within the fault depth parameter space, which is the focus of this study. Future work will also explore the fault length parameter space of the data and model, where the LW relationship can still be utilized.

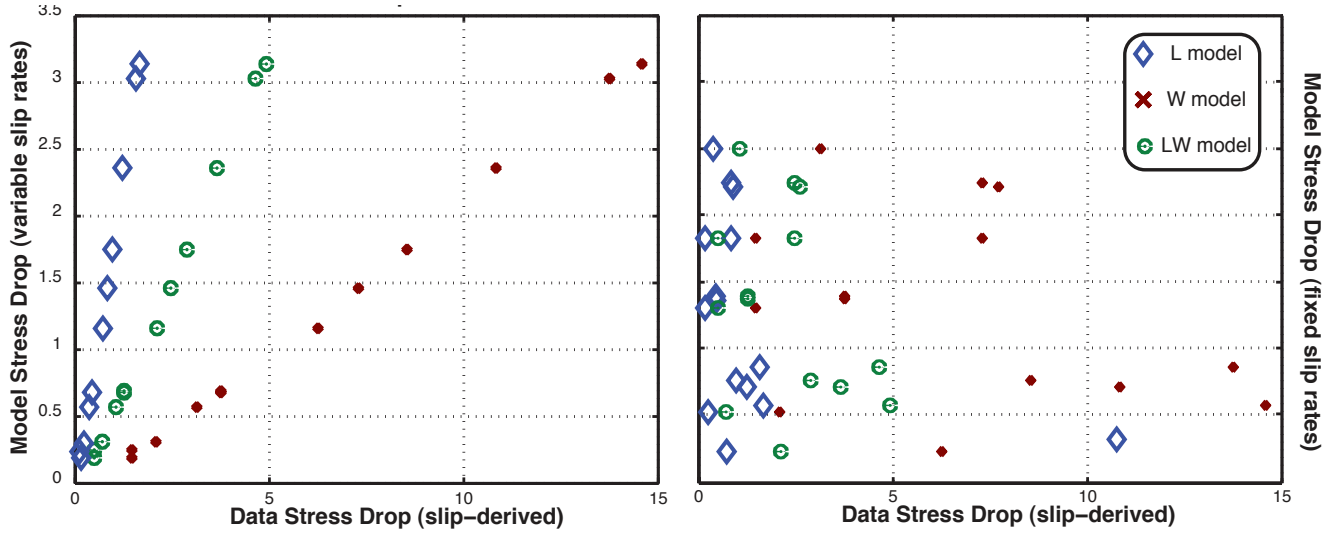

Figure 2.A.3. Data vs. model stress drop estimates. (a) Slip-derived paleoseismic stress drop using L, W, and LW relationships vs. model-derived stress drops assuming a variable slip rate. (b) Slip-derived paleoseismic stress drop using L, W, and LW relationships vs. model-derived stress drops assuming a fixed slip rate of 33 mm/yr.

Curriculum Vita

Teira Solis was born on a cold evening on October 17 of 1977 in Mexico City but was raised in Cd. Juarez. Daughter of journalist parents, she began pursuing a career in Sociology at the UACJ in Juarez. She married her high school sweetheart in 1998 and began a family.

In 2002 she moved to El Paso, TX with her family and in 2005 she started a new career in Geology at UTEP. The first few years at UTEP she was teaching environmental summer camps for children while working at the Center for Environmental Resource Management. She quickly became a well-known name in the department for her volunteering and her will to help everyone. This attitude earned her the Outstanding Geological Sciences Student of the year award in 2009. After receiving her Bachelors in Science degree in the winter of 2010 she started graduate studies under the guidance of Dr. Bridget Smith-Konter.

During the years as a graduate student, she received awards during national conferences and was the recipient of scholarships. In early 2012, she was a team member for the AAPG - Imperial Barrel Award and had the opportunity to represent the Southwest section at the International competition in Long Beach, CA. During the summer of 2012 she interned with Marathon Oil Company in Houston, TX as a Geophysicist. She has accepted a position at ConocoPhillips in Houston where she will be part of the Petrophysical Technology Organization.

Permanent address: 12099 Saint Romeo Ave.

El Paso, Texas. 79936

This thesis was typed by Teira Solis